ICW Note 1938
March 1989

nota

instituut voor cultuurtechniek en waterhuishouding, wageningen

A NEW SIMULATION MODEL OF BARE SOIL EVAPORATION IN ARID REGIONS (E V A D E S)

W.G.M. Bastiaanssen, P. Kabat and M. Menenti

LIST OF SYMBOLS

SYMBOL	INTERPRETATION	UNITS
a'	Apparent thermal diffusivity	$m^2.s^{-1}$
A	Amplitude	-
$b(h_m)$	Relative unsaturated hydraulic conductivity	-
c	Specific heat	$J.kg.K^{-1}$
C	Heat capacity	$J.m^{-3}.K^{-1}$
C	Solute concentration	$mol.l^{-1}$
$C(h_m)$	Differential soil water capacity	m^{-1}
C_p	Air specific heat at constant pressure	$J.kg.K^{-1}$
C_s'	Soil heat capacity	$J.m^{-3}.K^{-1}$
d	Dissociation factor	-
d	Zero-plane displacement	m
d	Damping depth	m
D	Diffusivity	$m^2.s^{-1}$
e_{sat}	Saturated vapour pressure	mbar
e_{act}	Actual vapour pressure	mbar
eff	Effective	-
FLXS	Transport flux	var.
g	Acceleration due to gravity	$m.s^{-2}$
g_a	Depolarisation factor	var.
$g(\tau)$	Surface roughness in combination with optical depth	-
G_0	Soil heat flux at the soil surface	$W.m^{-2}$
G_e	Soil heat flux at the evaporation front	$W.m^{-2}$
GWL	Groundwater level	m
H	Sensible heat flux	$W.m^{-2}$
H	Hydraulic head	m
h_m	Matric pressure head	m
h_{me}	Matric pressure head at the evaporation front	m
h_{osm}	Osmotic pressure head	m
h_{tot}	Total pressure head	m
k	Von Karman's constant	-
K	Specific permeability	m^2

SYMBOL	INTERPRETATION	UNITS
$K(h_m)$	Unsaturated hydraulic conductivity	$m.s^{-1}$
K_{sat}	Saturated hydraulic conductivity	$m.s^{-1}$
l_m	Mean molecular free path of water vapour	m
L	Latent heat of vaporization of water	$J.kg^{-1}$
LE_{act}	Actual evaporation	$W.m^{-2}$
LE_{pot}	Potential evaporation	$W.m^{-2}$
M	Molecular weight of water	$kg.mol^{-1}$
P	Total gas pressure	$N.m^{-2}$
P	Period	s
PHSA	Pressure head at surface level	m
q_v	Vapour flux	$kg.m^{-2}.s^{-1}$
q_l	Moisture flux	$m.s^{-1}$
q_p	Potential flux	$m.s^{-1}$
r	Mixing ratio	-
r_m	Pore radius	m
R	Resistance to transport	$s.m^{-1}$
Ray_{cr}	Critical Rayleigh number	-
Rd	Specific gas constant of dry air	$J.kg.K^{-1}$
Ri	Richardson number	-
R_n	Net radiation	$W.m^{-2}$
R_{sw}	Incoming shortwave radiation	$W.m^{-2}$
R_{swdf}	Diffuse shortwave radiatian	$W.m^{-2}$
Ru	Universal gas constant	$J.mol.K^{-1}$
Rv	Specific gas constant of water vapour	$J.kg.K^{-1}$
S	Slope of the saturation curve	$mbar.K^{-1}$
$S(h_m)$	Sink term	s^{-1}
t	Time	s
T	Temperature	K
T_e	Temperature at the evaporation front	K
T_0	Surface temperature	K
T_{lab}	Temperature at the laboratory during experiments	K
T_{vi}	Virtual temperature	K
u	Windspeed	$m.s^{-1}$
u*	Frictional velocity	$m.s^{-1}$
U	Relative humidity	-

SYMBOL	INTERPRETATION	UNITS
Vca	Convective flow velocity	$m.s^{-1}$
Vda	Diffusive flow velocity	$m.s^{-1}$
VPD	Vapour pressure deficit	mbar
W_e	Heat storage between surface/evaporation front	$W.m^{-2}$
W_{gwl}	Heat storage between evaporation front/groundwater	$W.m^{-2}$
z	Height or depth	m
z_e	Depth of the evaporation front	m
α_0"	Normalized surface reflectance	-
α_0	Surface reflectance	-
γ	Psychrometric constant	$mbar.K^{-1}$
δ	Variation of quantity	-
ϵ	Surface emissivity	-
ϵ'	Apparent emissivity of the atmosphere	-
ϵ	Ratio of molecular weight of water vapour and dry air	-
η	Viscocity	$N.s^{-1}.m^{-2}$
θ	Volumetric soil water content	m3.m-3
θ_e	Volumetric soil water content at the evap. front	$m^3.m^{-3}$
θ_{sat}	Total porosity	$m^3.m^{-3}$
λ	Soil dependant parameter	$m.s^{-0.5}$
λ_s*	Effective soil thermal conductivity	$W.m^{-1}.K^{-1}$
λ_s'	Apparent soil thermal conductivity	$W.m^{-1}.K^{-1}$
ρ	Density	$kg.m^{-3}$
τ	Shear stress	N
σ	Stefan Boltmann constant	$W.m^{-2}.K^{-4}$
σ_{wa}	Surface tension of water against air	$N.m^{-1}$
ϕ	Monin-Obukhov's function	-
ϕ_{su}	Sun zenith angle	-
Ω	Angular frequency	$rad.s^{-1}$
a	Air	-
cum	Cumulative	-
h	Heat	-
l	Liquid	-
m	Momentum	-
max	Maximum	-

SYMBOL	INTERPRETATION	UNITS
na	Halite	-
s	Soil	-
si	Quartz	-
v	Vapour	-
w	Water	-
x	Volumetric fraction of constituents	-

CONTENTS

1. INTRODUCTION

The rate of evapotranspiration of a cropped soil surface can be estimated with the aid of various simulation models. Most models describe the transport of water as a liquid medium across the entire soil profile, either one dimensionally (e.g. SWATRE, Feddes et al., 1978 and Kabat et al., 1989) or multidimensionally (e.g.UNSAT2, Neuman et al., 1975). Bare soil evaporation is hereby assumed to take place at soil surface level. The application of such models in hyper-arid regions like deserts and dry soils has to be questioned. The topsoil under these conditions can be extremely dry and vapour flow through the dry and often salty sandcrust may be the dominant transport process. Hence, existing simulation models, describing liquid transport towards the surface, can not be applied without major modifications.

The hydraulic conductivity as a transport process parameter in the dry range of soil water content relates to a transient mixture of liquid and vapour flow. Such an "effective" hydraulic conductivity is very difficult to measure with available laboratory techniques. An outcome is to establish a treshold for matric pressure head, below which one applies a Richard's-type equation to describe liquid flow, while above this treshold one should only consider vapour flow described by diffusion-type equations. Parameters of both type of equation have to consist of a permeability of the medium to vapour and to liquid flow. A theoretical concept of a liquid-vapour interface characterized by the critical matric pressure head i.e. evaporation front (Menenti, 1984) situated somewhere inside the unsaturated zone is briefly reviewed in this study.

A new finite difference one-dimensional transient numerical simulation model for bare soil EVAporation in DESerts (EVADES) has been developed. The model is written in Fortran 77 on the VAX/VMS version V4.5 operating system. The EVADES-model contains the Richard's equation for the movement of water in the liquid phase with its numerical solution scheme as applied in the SWATRE-model.

Above the vapour-liquid interface a vapour continuity equation of the Fick-type is applied. After establishing of the depth of the evaporation front, resistance factors for the transport of vapour and heat trough the soil profile are simulated in order to calculate the actual evaporation rate away from the surface by means of a combination equation.

In the framework of an evaporation study in the Western Desert of Egypt, vapour transport through the toplayer has to be assessed in order to predict natural losses of fossil groundwater. The new EVADES-model has been tested and validated with field data collected in the above mentioned regions.

2. SUMMARY OF THE SWATRE-MODEL

2.1. THEORETICAL ASPECTS OF THE EVAPORATION ESTIMATION IN THE SWATRE-MODEL

The SWATRE-model (Feddes et al., 1978 and Kabat et al., 1989) simulates transient one-dimensional water flow through the unsaturated/saturated zone, including water extraction by roots. The evaluation of the complete water balance is given at each time step. The applied upper boundary condition for bare soils is the maximum possible flux through the soil surface i.e. potential evaporation flux or infiltration. The actual flux through the soil surface in rainless areas is limited by the transport capacity of the soil matrix so that a flux regulation procedure is applied. Similarly, if the potential rate of infiltration exceeds the infiltration capacity of the soil, part of the water runs off, since the actual flux through the top layer is limited by moisture conditions in the soil.

$$/q(K,h_m)/ \leq /q_p/$$

$$h_{tot}^{lim} \leq h_m \leq 0$$

where: $q(K,h_m)$ = actual Darcian flux through the soil-air interface (evaporation or infiltration) determined by soil hydraulic properties (hm(θ)- and $K(h_m)$ relationship) ($cm.d^{-1}$)

q_p = the known potential surface flux (i.e. potential evaporation or infiltration) ($cm.d^{-1}$)

h_{tot}^{lim} = minimum allowed pressure head at the soil surface (matric and osmotic forces included) (cm)

h_m = actual matric pressure head at the soil surface (cm)

The limited value of the pressure head at the soil surface can be determined from equilibrium conditions between soil water and atmospheric vapour with the interface at the soil surface (Kelvin's law):

$$h_{tot}^{lim} = \frac{Ru\ T}{M\ g} \ln U \qquad (m) \qquad [1]$$

where Ru (8.314 $J.mol.K^{-1}$) is the universal gas constant, T (K) the absolute temperature, M (0.018 $kg.mol^{-1}$) the molecular weight of water, g ($m.s^{-2}$) the acceleration due to gravity and U (-) the relative air humidity. Hence, in case the soil is not evaporating potentially, a reduced flux (q_r) is considered to be the upper boundary flux. When the pressure head in the profile close to the soil surface, has the same order of magnitude as hm_{tot}^{lim}, the reduced evaporation flux (q_r) is expressed as a Darcian flux $q(K,h_m)$ through the upper topsoil. When the pressure head in the topsoil differs by order of magnitude comparing with h_{tot}^{lim}, a flux reducing procedure is involved based on the empirical model of Black and Gardner (1969):

$$E_{act} = \lambda\sqrt{t+1} - \lambda\sqrt{t} \qquad (mm.d^{-1}) \qquad [2]$$

where E_{act} ($mm.d^{-1}$) is the actual (reduced) evaporation flux for the drying period, λ($mm.d^{-0,5}$) is a soil dependent parameter and t (d) the time after the last day with a precipitation larger than 10 $mm.d^{-1}$. The actual soil evaporation flux rate is taken in the SWATRE-model as the minimum of the Darcian flux $q(K,h_m)$ and the flux E_{act}.

Non-steady water flow through the unsaturated porous soil, is based on the one-dimensional Darcy-equation in combination with the conservation of mass:

$$\frac{\partial h_m}{\partial t} = \frac{1}{C(h_m)} \frac{\partial}{\partial z} [K(h_m)(\frac{\partial h_m}{\partial z} + 1)] - \frac{S(h_m)}{C(h_m)} \qquad (cm.d^{-1}) \qquad [3]$$

where h_m (cm) is the soil-water (matric) pressure head, t (d) the time, $C(h_m)$ (cm^{-1}) the differential soil-water capacity at specific matric pressure head, z (cm) the depth, positive when directed upwards, $K(h_m)$ ($cm.d^{-1}$) the hydraulic conductivity at specific matric pressure head and $S(h_m)$ (d^{-1}) the water uptake by roots sink term at specific matric pressure head. This implicit second order partial differential equation is solved numerically by assuming linear gradients of matric pressure head versus time and depth between the nodes (Haverkamp et al., 1977).

The Thomas algorithm is applied to solve the finite difference scheme with explicit linearization of hydraulic conductivity and soil-water capacity for each time step (Remson, 1971).
An iteration procedure is applied within each variable time step with a convergence criterium allowing to simulate the real terms of water balance for any time period selected (Kabat et al., 1989).

The value of the pressure head at the soil surface can be treated in the model as Dirichlet type boundary condition (specified pressure head). The flux through the bottom of the profile can be given as input (Neuman type condition) or can be calculated from a relationship between bottom flux and groundwater level below surface and subsurface flow systems (Cauchy type condition)(Feddes et al., 1988). Eventually the depth of the groundwater table can be calculated. A prescribed pressure head at the bottom of the profile can be given as Dirichlet type boundary condition (zero matric pressure head at phreatic surface). For specific cases, a zero flux condition and free drainage can be used.

The potential evapotranspiration can be computed by means of several alternatives. Options for the application of semi-physical based equations of Penman and Monteith are built in. Also, empirically derived radiation equations like the equation proposed by Makking and by Priestly and Taylor belongs to the options. Values of evaporation and transpiration can be directly given as input to the model when known a priori.

2.2. COMMENTS ON THE APPLICATION OF THE SWATRE-MODEL IN ARID REGIONS

The land types in arid regions are characterized by mostly scarce vegetated and dry soils. When a shallow groundwater table is present, salt traces are often noticed. For example, the situation in the natural depressions of the Western Desert of Egypt are characterized by a flat, mainly non-vegetated, topography including a shallow groundwater table. The mean annual rainfall is less than 10 $mm.y^{-1}$. The surface consists of evaporites (halite) with a consequently high solute concentration in the bottom. The soil temperature shows a large diurnal oscillation and can be extremely high (upto 60°C).

The sink term of eq. [3] is to be neglected since the soil is mainly bare. The main complications on the application of the basic version of the SWATRE-model under hyper-arid bare soil conditions can be summarized as follows:

1. Motion of soil water is dominated by the large friction force between soil particles and water. The transport mechanism and the conditions under which it takes place can reach a magnitude of soil water content where the ability of the soil to conduct water in the liquid phase becomes asymptotically zero. It is intuitively clear that prevalent vapour displacement through the dry, sandy (eventually salt) crust will then be the major transport process. At such water content, the liquid diffusivity becomes less than the vapour diffusivity (Jackson et al., 1974) because the vapour diffusivity increases more with temperature than the liquid diffusivity does. So, vapour transport equations in the top layer have to be involved. The interface between vapour and liquid transport, i.e. evaporation front, can be found deep in the soil profile.
2. Empirical Eq. [2] does not hold true. Predictions of evaporation by means of this expression are reasonably accurate for short dry spells, which condition does not apply to desert climate.
3. When Eq. [2] is rejected, the actual evaporation will be taken as the Darcy flux through the top soil. The concept of a hydraulic conductivity in the very dry range is basically wrong when one consider it as a process directed ("effective") parameter, since the solid-vapour interaction is dominant over the solid-liquid interaction. The "effective" hydraulic conductivity in the dry range, is poorly measurable, so the application of such parameter under hyper-arid conditions has to be discussed with great attention. The current experimental knowledge of soil hydraulic conductivity in the dry range of soil water content has in this respect to be discussed. A proper fluid dynamic description of the process would involve a two-phase flow, thus describing the interactions between:
   - liquid and vapour
   - solid matrix and vapour
   - solid matrix and liquid

4. The matric pressure head gradient in this thin top layer is not very accurate, since pressure head at the soil surface is obtained by assuming equilibrium between atmospheric vapour pressure and vapour pressure in soil air.
   Small deviations from this equilibrium conditions cause large deviations in the pressure head gradient. Osmotic forces play another relevant role here, which is described more intensely in section 3.2.7. Hence, the Darcy flux through the top layer under dry conditions with possible osmotic effects is an educated guess.
5. From the surface energy balance equation it is known that net radiation (R_n) equals the sum of latent heat flux (LE), sensible heat flux (H) and the soil heat flux (G_0): $R_n+LE+H+G_0=0$. Since the soil heat exchange term (G_0) is for practical reasons not applied in the combination equations currently applied in the SWATRE-model, an error in the determination of the latent heat flux is introduced. The soil heat exchange has to be theoretically subtracted from the net radiation, with less radiation energy available for latent and sensible heat fluxes. Under dry conditions and absence of vegetation, soil heat flux is a large fraction of the net radiation (10-35 %).
6. The actual temperature and solute concentration of soil water may be different from pure water at 20° C (laboratory conditions). The resulting changes in the bulk properties of soil water will deeply modify the analyzed soil hydraulic properties $h_m(\theta)$ and $K(h_m)$ in the labaratory. Hence, corrections have to be applied to the measured hydraulic relationships.
7. When calculation of the actual latent heat flux in small time steps has to be carried out, hourly values of potential evapotranspiration are required. An option to calculate the hourly meteorological variables for cases where meteorological data sets are incomplete, is not implemented in the current SWATRE-model.

Because of the above mentioned considerations, it was deemed necessary to design a new simulation model using the Richard's equation with its finite difference numerical solution scheme, but including the necessary improvements in the physics of transport processes between the evaporation front and the soil surface.

3. MECHANISMS OF LIQUID, VAPOUR AND HEAT TRANSPORT IN UNSATURATED SOILS

3.1. DETERMINATION OF ACTUAL EVAPORATION

3.1.1. Actual evaporation from a drying bare soil

Soil evaporation is potential when the soil does not restrict liquid flow towards the evaporation sites. However, at windy locations with a high soil temperature and absence of rainfall, the top layer can be very dry (< 0.03 $cm^3.cm^{-3}$) e.g. the encrusted top soil in the Western desert of Egypt.

Water will no longer evaporate directly from the soil surface. A liquid-vapour interface or so called evaporation front is situated then inside the

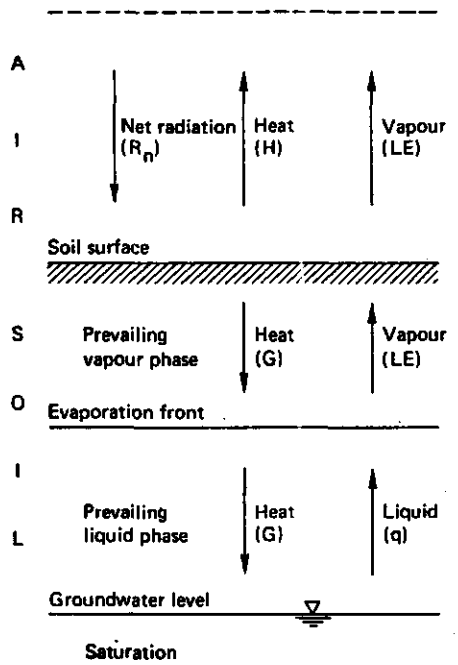

Fig. 1 Schematic representation of the presence of an evaporation front inside a dry topsoil. The directions of vapour and heat flow are indicated for the midday situation, where R_n is the net radiaton, LE the latent heat flux, H the sensible heat flux, G the soil heat flux and q the Darcy flux

soil profile. Under these conditions, the interrelation of vapour and heat transfer through unsaturated soil must be theoretically described.
Vapour transport through air filled pores is the dominant mass transport process above the evaporation front. Water in the liquid phase represents the main contribution to mass transfer through water filled pores under the evaporation front. Theories underlying the transition from liquid to vapour flow and a definition of the evaporation front are outlined in section 3.1.2. The heat and vapour flow through the air filled pores above the evaporation front are coupled. This procedure is associated with conductive heat flow, thermal convection of soil air and gas diffusion transport. Since water is per definition released at the evaporation front and the heat wave penetrates from the soil surface, the flow directions of heat and vapour through the soil can be contrary during long spells of the day. The required latent heat at the evaporation front is released from the soil heat flow, which drives the vapour flow upwards.

3.1.2. Definition of the evaporation front

Preliminary, a definition of the liquid-vapour interface or so called evaporation front as proposed by Menenti (1984) will be briefly recalled. Fick's law for the diffusion of gases remains only valid in pores having a radius (r_m) much larger than the mean free-path of a water vapour molecule (l_m). Einstein's random-walk theory shows that gas-gas collisions will take place in this pores ($r_m > l_m$). The mean free-path of water vapour is dependent on temperature as:

$$l_m = \left(\frac{(T-7)}{50}\ 1.3 + 4.0\right) \qquad (10\text{-}8\ m) \qquad [4]$$

where l_m (m) is the mean free path of a water vapour molecule and T (°C) the temperature. With decreasing pore size, Fick's molar flow will gradually change to Knudsen- and film flow ($r_m < l_m$). Under gas flow regime of the Knudsen type, vapour flow becomes equal to the mean molecular velocity (water vapour: 565 $m.s^{-1}$), so that the probability of reentering a particular pore is small.
The mean molecular velocity is much larger than the diffusion velocity. Thus the air-liquid water interface (meniscus) in pores having $r_m = l_m$ is

unstable. When the meniscus reach this radius ($r_m = l_m$), the evaporation rate will increase from the meniscus. So there will be a rapid transition from a condition where pores with $r_m > l_m$ are water-filled to the case of pores with $r_m < l_m$ being air filled. This process will give a sharp transition of soil water content with depth. To support interpretation, it was indicated by Philip (1957) that the ratio of vapour flux (q_v) to liquid water flux (q_l) increases rapidly above this transition zone. Jackson declared later (1964, 1974) that the vapour diffusivity becomes even higher than the liquid diffusivity. The particular threshold of matric pressure head (h_m) or water content where $r_m = l_m$ can be expressed as the soil water content at the evaporation front (θ_e). A definition of this transition layer can now be given on the basis of the relationship between pore radius, matric pressure head and soil water content. The matric pressure head at the depth of the evaporation front (z_e) where $r_m = l_m$ can be calculated as:

$$h_{me} = \frac{1}{\rho_w g} \frac{2 \sigma_{wa}}{l_m} \quad (m) \qquad [5]$$

where h_{me} = matric pressure head at the evaporation front (m)
ρ_w = local density of liquid water ($kg.m^{-3}$)
σ_{wa} = local tension of water against air ($N.m^{-1}$)
l_m = mean free path of a watermolecule (m)
g = acceleration due to gravity ($m.s^{-2}$)

Values of the physical properties of water can be found in appendix 5 and 6. Theories underlying variation of these properties are presented rather extensively in section 3.2.8.
From the vertical matric pressure head distribution ($h_m(z)$) and the matric pressure head at the evaporation front (h_{me}), the depth of the evaporation front (z_e) can be located as that $z_e = z$ where $h_m(z) = h_{me}$. The soil water content at the evaporation front (θ_e) can then be obtained through the $h_m(\theta)$-relationship.

3.1.3. Menenti's combination equation

The basic principles underlying Menenti's combination equation (eq. [6]), is the internal soil evaporation process combination with the radiation and

flux terms at the soil surface. The derivation of eq. [6] is presented in appendix 1. To evaluate the evaporation flux at time steps less than one day, a term accounting for heat storage between the surface and the evaporation front has been added to the original equation. The fluxes are considered positive when reaching the surface.

$$LE = - \frac{\rho_a C_p [e_{sat}(z) - e_{act}(z)] + S_a R_{ah}(R_n + G_e + W_e) + S_s \rho_a Cp R_{sh} (G_e + W_e)}{\gamma(R_{av} + R_{sv}) + S_a R_{ah} + S_s \rho_a C_p R_{sh}} \quad [6]$$

where

LE	= Latent heat flux	$(W.m^{-2})$
ρ_a	= Air density	$(kg.m^{-3})$
C_p	= Air specific heat at constant pressure	$(J.kg^{-1}.K^{-1})$
e_{sat}	= Saturated air vapour pressure	(mbar)
e_{act}	= Actual air vapour pressure	(mbar)
S_a	= Slope of the saturated air vapour pressure curve	$(mbar.K^{-1})$
S_s	= Slope of the saturated soil vapour pressure curve	$(mbar.K^{-1})$
R_{ah}	= Air resistance to heat transfer	$(s.m^{-1})$
R_{sh}	= Soil resistance to heat transfer	$(W^{-1}.m^2.K)$
R_{av}	= Air resistance to vapour transfer	$(s.m^{-1})$
R_{sv}	= Soil resistance to vapour transfer	$(s.m^{-1})$
R_n	= Net radiation	$(W.m^{-2})$
G_e	= Soil heat flux at the evaporation front	$(W.m^{-2})$
G_0	= Soil heat flux at the surface	$(W.m^{-2})$
W_e	= Heat storage between surface and evap. front	$(W.m^{-2})$
γ	= Thermodynamic psychrometric constant	$(mbar.K^{-1})$

Resistance factors for the transport of vapour (R_{sv}) and heat (R_{sh}) between the evaporation front and the soil surface have to be taken into account (Fig. 2). The applied procedure in our model is to simulate the depth of the evaporation front, according the theories of section 3.1.2 and 3.1.4 respectively, whereafter the evaporation can be computed by means of eq. [6].

When the evaporation front is situated at surface level, the resistance factors R_{sv}, R_{sh} equals zero. For a zero depth of the evaporation front and with the assumption $R_{sv} = R_{ah}$, the combination equation coincides with commonly accepted potential evaporation formulae (e.g. Penman 1948, v. Bavel 1966).

When the evaporation front is located inside the soil profile, the actual evaporation is governed by meteorological and soil physical parameters as

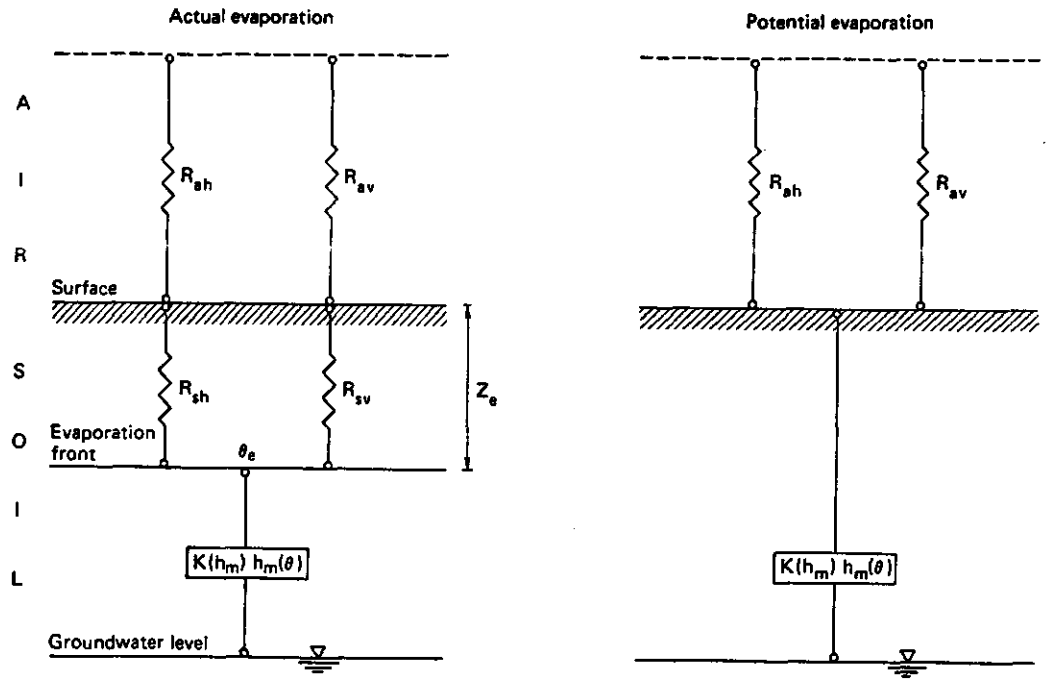

Fig. 2 Schematic representation of the resistances (R) to heat (h) and vapour (v) flow in air (a) and soil (s). The depth of the evaporation front (z_e) depends on the soil moisture contribution in the profile, i.e. on hydraulic properties like hm(θ)- and $K(h_m)$ relationships

well. The deeper the evaporation front, the higher the resistance factors. Further it can be mentioned that the R_{sv}-value are physically analogous to the internal crop resistance when considering a canopy layer as proposed by Monteith (1965). For a detailed description of the

Table 1. Outine of the parameters required for the combination equation (eq. [6]) as presented elsewhere in this report

Parameter	Section	Equation
R_{sh}, R_{sv}	3.1.4	7, 8, 12, 13, 16, 17
G_e, W_e	3.1.5	19, 20, 21
e_{sat}	3.2.5	36
e_{act}	3.2.7	50
R_n	appendix 2	77
S_a, S_s	appendix 2	81
R_{ah}, R_{av}	appendix 3	88, 89, 92, 93

Penman- v. Bavel expression, one is refered to appendix 2.
Table 1 presents an overview with the references of all terms required for eq. [6] as described in the present report.
Field observations showed the presence of a daily cyclus of deposition and successive evaporation of dew. This form of latent heat exchange occurs early in the morning. Consequently, a temporary second evaporation front is present. Generally, the second evaporation front will disappear through the course of the day. The same evaporation theory should be applicable.

3.1.4. Soil resistances to heat and vapour flow

As illustrated in Fig. 2, resistance factors for the transport of vapour (R_{sv}) and heat (R_{sh}) through the soil have to be considered.
The next step is to describe the dynamic processes in relation with the resistance factors above the evaporation front. The procedure is composed of three cases:

(A) evaporation takes place at the soil surface (potential evaporation)
(B) evaporation takes place at the evaporation front, with diffusive transport of water vapour between the evaporation front and the soil surface (actual evaporation)
(C) evaporation takes place at the evaporation front, with thermal convection of moist soil air i.e. free convection between the evaporation front and the soil surface (actual evaporation)

Case (A): When the evaporation site is at surface level, the limit of the depth of the evaporation front equals zero:

$$\lim_{z_e \to 0} (LE_{act}) = LE_{pot}$$

The evaporation rate is governed by the micro-meteorological conditions rather than by soil physical properties. Hence, there is no resistance for transport between the phase transition zone and the evaporation site.

solution: $R_{sh} = 0.0$ $(W^{-1}.m^2.K)$ [7]

$R_{sv} = 0.0$ $(s.m^{-1})$ [8]

Case (B): The transport coefficients in the top soil play a role for the estimation of the actual evaporation flux. The liquid transport capacity above the evaporation front ($\theta < \theta_e$) is limited and may be neglected. Air filled pores above the evaporation front contain moist soil air i.e. a mixture of dry air and water vapour. The vapour pressure at the evaporation front is nearly saturated, while the relative humidity near the soil surface is much lower. Gradients in vapour density can be related with the gradients of temperature (thermal vapour diffusion) and soil water content (iso-thermal vapour diffusion). This can be combined to obtain the distribution of vapour density or the so called abolute humidity ($kg.m^{-3}$), according eq. [9]:

$$\frac{\partial \rho_v(\theta,T_s)}{\partial z} = \frac{\partial \rho_v(\theta)}{\partial T_s}\frac{\partial T_s}{\partial z} + \frac{\partial \rho_v(T_s)}{\partial \theta}\frac{\partial \theta}{\partial z} \qquad (kg.m^{-4}) \qquad [9]$$

The vapour flux equation can be written as an ordinairy Fick-type vapour diffusion equation, describing the vapour flow by means of an "effective" molecular diffusion coefficient (D_{eff}) of water vapour in moist soil air:

$$q_v = - D_{eff}\frac{\partial \rho_v(\theta,T_s)}{\partial z} \quad \text{or} \quad q_v = - D_{eff}\frac{\delta \rho_v}{z_e} \qquad (kg.m^{-2}.s^{-1}) \qquad [10]$$

In section 3.2.5 it will be shown that vapour flux can be related with the apparent soil thermal conductivity (λ_s'). Latter parameter takes into account the overall effect of heat conduction and heat convection (see eq. [37]).
The vapour flux can be expressed as a vapour diffusion velocity too (eq. [11]), which can vice versa be applied to obtain the vapour flux from the vapour diffusion velocity. With the gradient of vapour density known, D_{eff} can then be derived.

$$LE = - L\, q_v = - L\rho_v\, Vda \qquad (W.m^{-2}) \qquad [11]$$

solution: $$R_{sh} = z_e/\lambda_s' \qquad (W^{-1}.m^2.K) \qquad [12]$$

$$R_{sv} = z_e/D_{eff} \qquad (s.m^{-1}) \qquad [13]$$

Case (C): Onset of thermal convection is likely when the Rayleigh number is higher than a treshold value of the Rayleigh number with correspondave

boundary conditions (MENENTI, 1984).
Otherwise the density driven flow of vapour in moist air is a diffusive transport process (case B). When thermal convection of moist soil air takes place, the latent heat flux can be expressed in the following form:

$$LE = - L\, q_v = - L\, \rho_v\, Vca \qquad (W.m^{-2}) \qquad [14]$$

where Vca ($m.s^{-1}$) is the mean convective velocity of soil air. In order to establish in this situation the physical meaning of R_{sv}, the term "effective" vapour diffusivity (D_{eff}) is again introduced, where the convective soil air motion is rearranged into an "effective" diffusive transport phenomenon of the Fick-type:

$$\rho_v\, Vca = - D_{eff}\, \frac{\delta \rho_v}{z_e} \qquad (kg.m^{-2}.s^{-1}) \qquad [15]$$

solution: $R_{sh} = z_e/\lambda_s'$ $\qquad (W^{-1}.m^2.K)$ $\qquad [16]$

$$R_{sv} = z_e/D_{eff} \qquad (s.m^{-1}) \qquad [17]$$

The preceding discussions and criteria can be summarized as in table 2: A schematic representation is depicted in Fig. 3. For details, one is refered to section 3.2.6.

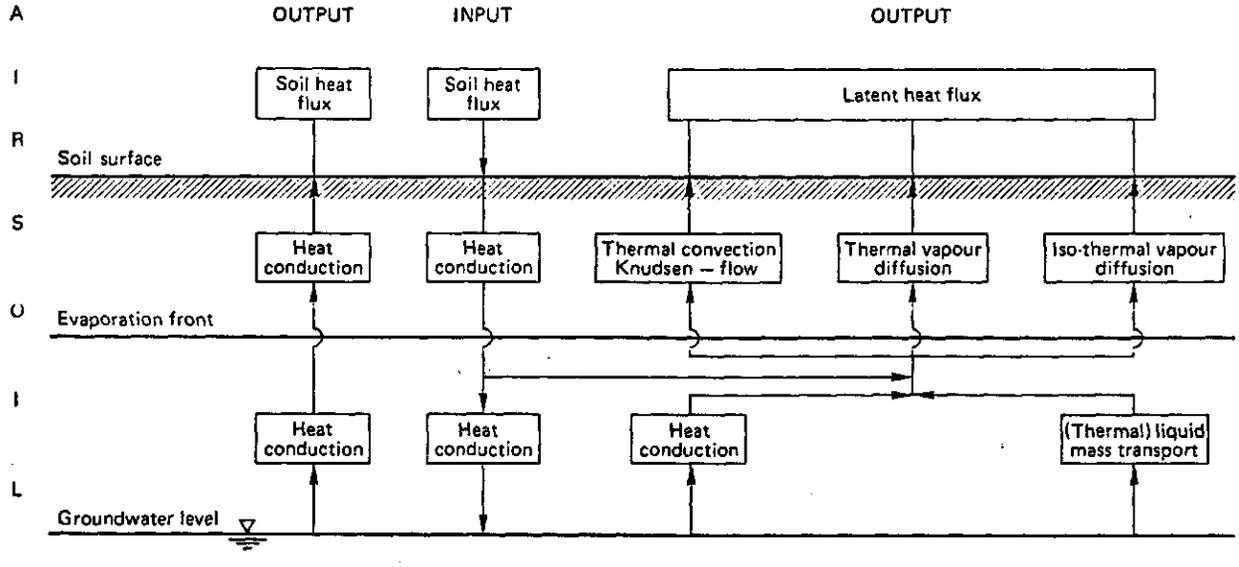

Fig. 3. Schematic representation of possible heat flow processes in the unsaturated zone

Table 2. Overview resistance to transport of heat and vapour in soil

transport	z_e (cm)	evapo-ration	$\partial\rho v/\partial z$ ($kg.m^{-4}$)	Rayleigh (-)	λ_s' ($W.m^{-1}.K^{-1}$)	D_{eff} ($m^2.s^{-1}$)	R_{sh} ($s.m^{-1}$)	R_{sv} ($s.m^{-1}$)
	0	pot.	0	$< Ray_{cr}$	-	-	0.0	0.0
free conv.	> 0	act.	> 0	$> Ray_{cr}$	$f(\lambda_s^*, Vca)$	$Vca, \partial\rho_v/\partial z$	z_e/λ_s'	z_e/D_{eff}
diff.trans.	> 0	act.	> 0	$< Ray_{cr}$	$f(\lambda_s^*, Vda)$	$Vda, \partial\rho_v/\partial z$	$z_e/\lambda s'$	z_e/D_{eff}

3.1.5. Soil heat flux at the soil surface

The heat flux penetrating a bare soil surface (G_0) reduces with depth since heat will be accumulated along the profile. Heat storage (W_e) reduces the downwelling heat wave from the surface (damping effect). Hence, the heat flux entering the evaporation front (G_0-W_e) differs from the heat flux penetrating the soil surface (G_0). The net energy reaching the evaporation front is used for both the evaporation process (LE) and heat flux between the evaporation front and the groundwater table (G_e). Figure 4 illustrates the distribution of the energy flux from the soil surface.
The soil heat flux penetrating the soil surface can be empirically related with net radiation (BASTIAANSSEN, 1988b). It was shown that the ratio G_0/R_n varies with soil thermal diffusivity and surface reflectance. This is a practical solution for cases where no measurements of G_0 are available. The expression is based on field work carried out in the mainly non-vegetated Qattara depression. The measured thermal diffusivity varied between 0.25 and 0.55 10^{-6} $s.m^{-1}$.

$$G_0/R_n = (0.84\ \alpha_0"-0.35).(p-\sqrt{p^2-4pp}) \qquad (-) \qquad [18]$$

with $p = 0.995\ a' - 0.185$

$pp = 0.179\ a'^2 - 0.14\ a'$

where a' = soil thermal diffusivity ($10^{-6}\ m^2.s^{-1}$)

$\alpha_0"$ = normalized surface reflectance (-)

The physical meaning of soil thermal diffusivity and the normalized surface reflectance are discussed in paragraph 3.2.5 and appendix 2 respectively. The importance of eq. [18] is evident for the estimation of G_e and W_e since both variables has to be known in order to solve eq. [6].

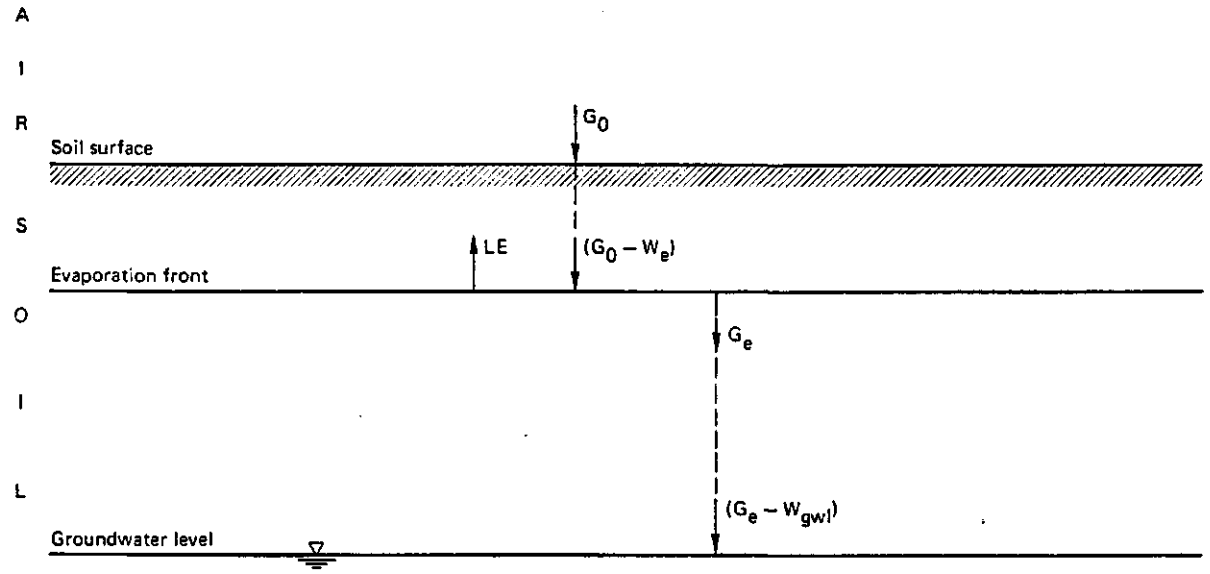

Fig. 4. Distribution of the energy penetrated from the soil surface at midday. Heat storages (W_e, W_{gwl}), latent- (LE) and soil heat fluxes (G_0, G_e) are taken into account

Although G_e and W_e can be derived seperately by eq. [20] and [21], it is desirable to apply a energy balance procedure as expressed with eq. [19]. Otherwise, temperature values may effect the determination of W_e- and G_e-values too much. If for instance the evaporation front is near the soil surface, large gradients of temperature results immediately in highly sensitive quantaties of W_e and G_e. If the assessed sum of W_e and G_e from eq. [20] and [21] is larger than G_0, the flux will be limited by the energy balance equation at the evaporation front (eq. [19]). Fluxes in the direction of the evaporation front are considered positive.

$$G_0 - W_e + LE + G_e = 0 \qquad (W.m^{-2}) \qquad [19]$$

$$W_e = \int_0^{z_e} C_s \frac{\partial T_s}{\partial t} dz \quad \text{if} \quad /W_e/ < /(G_0 - LE - G_e)/ \qquad (W.m^{-2}) \qquad [20]$$

$$G_e = -\lambda_s' \frac{\partial T_s}{\partial z} \quad \text{if} \quad /G_e/ < /(G_0 - LE - W_e)/ \qquad (W.m^{-2}) \qquad [21]$$

3.2. COUPLED PHYSICAL PROPERTIES IN THE TOPSOIL

3.2.1. Soil thermal properties

Soil heat exchange is dependent on the thermal properties of the different soil constituents. The non-steady volumetric fraction of water and air can be used to obtain variable heat capacity and heat conductivity figures i.e. the associated heat-water flow. Table 3 gives some values of the thermal properties of the soil components.

Table 3. Thermal properties of main soil particles (T=10°C) (after MENENTI, LUPINI and ALIVERTI, 1979)

Substance	Thermal conductivity ($W.m^{-1}.K^{-1}$)	Specific heat ($J.kg^{-1}.K^{-1}$)	Density ($kg.m^{-3}$)
Quartz	8.832	758.1	2660
Water	0.575	4186.0	1000
Air	0.025	1004.0	1.25
Organic matter	0.245	1938.0	1300
Clay	2.905	758.1	2650
Halite	5.750	412.6	2180

The soil heat capacity (C_s) is the product of density (ρ_s) and specific heat (c_s), where the soil has to be regarded as a composition of the given constituents. The soil heat capacity of the system can be computed as the weighted mean of the heat capacities of the different soil constituents:

$$C_s = (\rho c)_s = (x_{si}\ \rho_{si}\ c_{si} + x_w\ \rho_w\ c_w + x_a\ \rho_a\ c_a + x_{na}\ \rho_{na}\ c_{na}) \qquad [22]$$

where C = heat capacity ($J.m^{-3}.K^{-1}$)
c = specific heat (see table 2) ($J.kg^{-1}.K^{-1}$)
ρ = density (see table 2) ($kg.m^{-3}$)
x = volumetric fraction of each soil constituent ($cm^3.cm^{-3}$)
quartz (si), water (w), halite (na), air (a)

The high thermal conductivity of quartz and its abundant presence in sandy soils requires for a more detailed temperature (°C) dependent description (after International Critical Tables):

$$\lambda_{si} = 8.57 - \left[\frac{(T_s-20)}{55}\ 1.47\right] \qquad (W.m^{-1}.K^{-1}) \qquad [23]$$

3.2.2. Heat balance equation

The general one-dimensional heat balance equation, without radiation term, heat sources and sinks for a homogeneous soil layer reads:

$$(\rho c)_s \frac{\partial Ts}{\partial t} = \lambda_s^* \frac{\partial^2 T_s}{\partial z^2} - (\rho c)_f\ Vca \frac{\partial T_s}{\partial z} \qquad (W.m^{-3}) \qquad [24]$$

where $(\rho c)_s$	= Soil heat capacity	$(J.m^{-3}.K)$
$(\rho c)_f$	= Fluid heat capacity	$(J.m^{-3}.K)$
λ_s^*	= Isotropic "effective" heat conductivity	$(W.m^{-1}.K^{-1})$
Vca	= Convective flow velocity	$(m.s^{-1})$
T_s	= Temperature	(K)
t	= Time	(s)
z	= Vertical distance	(m)

The first term on the right hand side describes the conductive heat transport through the porous soil medium when no fluid convection takes place, while the second term on the right hand side accounts for the convective heat transport with moist soil air being the fluid. The procedures to describe the conductive heat and convective heat flow are anticipated in section 3.2.4. and 3.2.5. respectively.

The convective vapour displacement will increase the total transport of heat through the unsaturated region. The required experimental data to describe properly the microphysical aspects of convective flow as described in Eq. [24] are seldom available.
Therefore, the explicit description of convective flow is often omitted and substituted by the conduction-like balance equation, introducing an apparent conductivity term:

$$(\rho c)_s \frac{\partial T_s}{\partial t} = \lambda_s' \frac{\partial^2 T_s}{\partial z^2} \qquad (W.m^{-3}) \qquad [25]$$

where λ_s' (W.m.K-1) is the apparent heat conductivity of the soil. The apparent heat conductivity accounts for the conductive and convective heat transport as well. Changes of latent heat at the liquid-vapour interface may be conceived as a sink term in the heat balance equation under the evaporation front.

3.2.3. Temperature distribution in the soil profile

A time dependent one-dimensional soil temperature profile can be obtained from the solution of the soil heat balance equation (eq. [25]). Two phenomena play an important role on the periodical temperature fields; the damping effect and the phase shift of the heat wave. An analytical solution for the heat balance equation with a sinusoidal function of the upper boundary condition at z = 0 was given by Carslaw and Jaeger (1959). If the average periodical surface temperature equals the average periodical soil temperature at each depth, the temperature function becomes for homogeneous soils:

$$T_s(z,t) = \overline{T}_0 + A(0)\, e^{-z/d} \sin(\Omega t - z/d) \quad \text{with} \quad (K) \qquad [26]$$

$$d = (2\, a'/\Omega)^{0.5} \quad \text{and} \quad (m) \qquad [27]$$

$$\Omega = 2\, \pi/P \qquad (rad.s^{-1}) \qquad [28]$$

where $T_s(z,t)$ = Soil temperature at time t and depth z (K)
$\overline{T}_0$ = Average surface temperature for period P (K)
$A(0)$ = Amplitude of surface temperature (K)
z/d = Phase shift of temperature wave (-)
d = Damping depth (m)
a' = Apparent thermal diffusivity ($m^2.s^{-1}$)
Ω = Angular frequency ($rad.s^{-1}$)
P = Period (s)

The only way to verify predicted values of soil temperature, are on site soil temperature observations. Fieldwork in the Qattara depression showed

that the apparent thermal diffusivity varies with depth (Bastiaanssen, 1988b). The heterogeneity can be explained by the stratified water content, varying salt aggregates and presence of cracks. The heat flow through gas filled pores is hereby an entangled process. A different explanation is that the curvature of the measured sinoide between day and night time is different (Fig. 5). An alternative solution was found by combining measured soil temperature amplitudes in the depth-domain with sinusoidal temperature regimes in the time-domain. The daily cyclus is split up into two different periods:

$$T_s(z,t) = \overline{T}_s(z) + A1(z)\ \sin[(\pi t/P1)] \quad \text{when } T_s(z,t) \geq \overline{T}_s(z) \quad (K) \quad [29]$$

$$T_s(z,t) = \overline{T}_s(z) - A2(z)\ \sin[(\pi t/P2)] \quad \text{when } \overline{T}_s(z,t) \leq T_s(z) \quad (K) \quad [30]$$

where $\overline{T}_s(z)$ (K) is the daily average temperature at depth z, Ax(z) the temperature amplitude of the period considered and P_x the total period between the moments of the time where $T_s(z,t) \geq \overline{T}_s(z)$ and $T_s(z,t) \leq \overline{T}_s(z)$. Note that this trick involves two different amplitudes and periods (Fig. 5) for one daily cyclus. In this form, the function is not a depth related problem anymore, so that difficulties around the heat damping proces are evaded. As a matter of fact, temperature values for each depth and time step can be established when the temperature amplitudes are observed and the average temperature can be estimated. Similar types of equation will be applied for the air temperature, global radiation and relative humidity during day and nighttime as well.

An approach with sinusoidal function against time are outlined in appendix 4. It is logical that this type of functions are only validated when clouds are absent so that the cyclus of the net radiation and consequently surface temperature is sinusoidal.

3.2.4. Heat conduction in soil according to de Vries model

Heat conduction in soils is the mechanism where heat transfer takes place by transfering kinetic energy of the molecules.

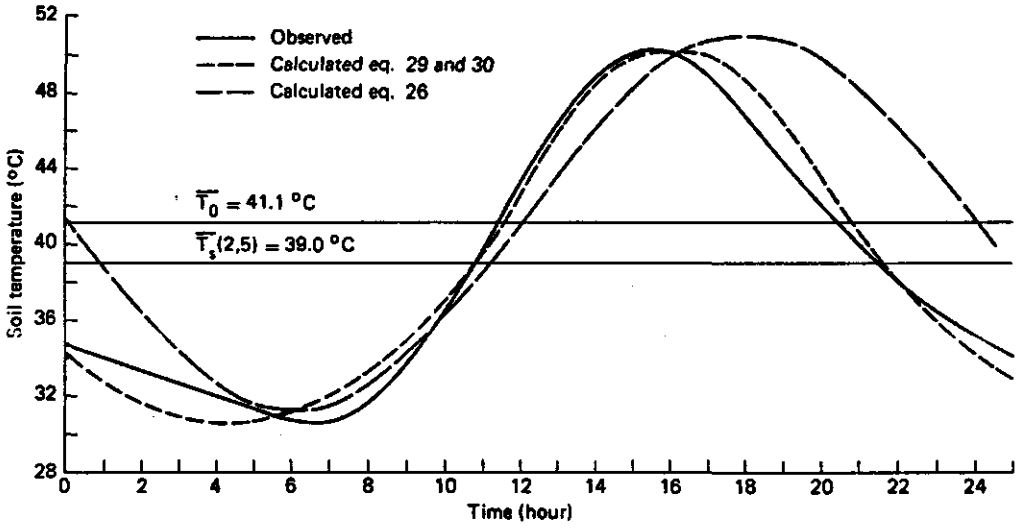

Fig. 5. Observed and calculated diurnal variation of soil temperature in a salty sandy topsoil (2.5 cm) at Bir Qifar in the Western Desert of Egypt, 18/19 June 1988. The considered period is one day.

The mean "effective" thermal conductivity per unit volume of soil (λ_s*), can be derived from the different constituents being water (w), quartz (si), halite (na) and air (a) according to de Vries (1963):

$$\lambda_s^* = \frac{u_w x_w \lambda_w + u_{si} x_{si} \lambda_{si} + u_{na} x_{na} \lambda_{na} + u_a x_a \lambda_a}{u_w x_w + u_{si} x_{si} + u_{na} x_{na} + u_a x_a} \qquad (W.m^{-1}.K^{-1}) \quad [31]$$

where u (-) is the ratio of the average temperature gradient in soil particles to the corresponding gradient in the surrounding medium and x ($cm^3.cm^{-3}$) the volumetric fraction of each soil constituent.
The volumetric fraction of quartz is equal to the inverse porosity minus the volumetric fraction of salt aggregates.

The determination of u is difficult due to two reasons:

1. The ratio of temperature gradients can only be estimated under the assumption that heat flux is the same in both materials, which is not necessarily true.
2. It is very difficult to obtain accurate experimental data on this process.

Equations to obtain u can be given with the following restrictions (table 4)

- the soil particles are ellipsoidal shaped

Table 4. Expressions for the ratio of thermal gradients of soil particles in relation with their neighbouring medium

	Surrounding medium air	Surrounding medium water
u_w	$\frac{1}{3}\left(\frac{2}{1+\lambda_w/\lambda_a\ g_a} + \frac{1}{1+\lambda_w/\lambda_a\ (1-2g_a)}\right)$	1.0
u_{si}	$\frac{1}{3}\left(\frac{2}{1+\lambda_{si}/\lambda_a\ g_a} + \frac{1}{1+\lambda_{si}/\lambda_a\ (1-2g_a)}\right)$	$\frac{1}{3}\left(\frac{2}{1+\lambda_{si}/\lambda_w\ g_a} + \frac{1}{1+\lambda_{si}/\lambda_{wi}(1-2g_a)}\right)$
u_{na}	$\frac{1}{3}\left(\frac{2}{1+\lambda_{na}/\lambda_a\ g_a} + \frac{1}{1+\lambda_{na}/\lambda_a\ (1-2g_a)}\right)$	$\frac{1}{3}\left(\frac{2}{1+\lambda_{na}/\lambda_w\ g_a} + \frac{1}{1+\lambda_{na}/\lambda_w\ (1-2g_a)}\right)$
u_a	1.0	$\frac{1}{3}\left(\frac{2}{1+\lambda_a/\lambda_w\ g_a} + \frac{1}{1+\lambda_a/\lambda_w\ (1-2g_a)}\right)$

- the axes a, b and c of the ellipsoidal particles are orientated in a random way
- a specific particle will not affect the temperature distribution of its surrounding particles

Furthermore, it should be noted that the choice of one constituent as "the continuous surrounding medium" depends on the volumetric water content. In the EVADES-model, the soil water content at the evaporation front is applied as the treshold value, since the soil water content above the evaporation front is rather small and constant. Below this treshold of moisture content, air is considered as being "the continuous surrounding medium".

When the soil remains saturated, the shape factor of the ellipsoid in direction of the a-axis (g_a) is considered to be spherical i.e. $g_a = 0.333$. With decreasing water content, g_a can be evaluated upto the water content at the evaporation front by means of a linear interpolation between the maximum value, $g_a = 0.333$ and minimum value, $g_a = 0.035$ (De Vries, 1963):

$$g_a = 0.035 + (0.333-0.035)\frac{(\theta_{act}-\theta_e)}{(\theta_{sat}-\theta_e)} \quad (-) \quad \theta_e \leqslant \theta_{act} \geqslant \theta_{sat} \qquad [32]$$

Below the threshold, with a discontinuity of g_a, the calculations with air being the surrounding medium can be done according eq. [33]. This is impor-

tant for the derivation of the effective soil heat conductivity above the evaporation front.

$$g_a = 0.013 + (0.098 - 0.013) \frac{\theta_{act}}{\theta_e} \quad \theta_{act} \leq \theta_e \quad (-) \qquad [33]$$

3.2.5. Heat convection in soil

Heat convection in soil is the mechanism where heat transfer takes place by liquid and vapour transport. Free and forced convection has to be distinghuished. Free or thermal convection occurs when temperature gradients cause air movement. This is different from the so called thermally induced vapour flux, which is a vapour diffusion transport process induced after temperature gradients (see case B, section 3.1.4). Forced convection of heat only occurs when frictional forces like wind induces a heat flow transport.

A rule of thumb is that free or thermal convection will certainly occur when the air flow velocity becomes larger than twice the speed of vapour diffusion i.e. faster than $2.5\ 10^{-3}$ $m.s^{-1}$ (see case C, section 3.1.4).

Soil air convection and diffusive vapour movement are heat transfer enhancements superposed on the conductive heat flow. Differences in vapour density cannot be obtained directly from soil temperature only (see eq. [9]).

A driving buoyancy force exist above the evaporation front since density of soil air decreases with increasing humidity. The density of soil air at the evaporation front is lower than at the soil surface most of the time, because the molecular weight of water vapour is smaller (18 $gr.mol^{-1}$) than of dry air (29 $gr.mol^{-1}$) at the same pressure and temperature. Moist air is a gas mix ture consisting of dry air with water vapour. The contribution of the actual vapour pressure (e_{eact}) and the total pressure of moist air (P) has to be considered. Temperature of moist soil air has to be converted first into an equivalent temperature, the so called virtual temperature. Virtual temperature is the temperature of dry air when it has the same density as moist air at a constant total pressure of moist air.

Then, gradients in virtual temperature will directly yields density gradients of soil air. The virtual temperature is calculated as:

$$T_{vi} = \frac{(1 + \tilde{f}/\epsilon)}{1 + \tilde{f}} T_s \qquad (K) \qquad [34]$$

where $\tilde{f}$ (-) is the mixing ratio i.e. the ratio between the mass of vapour in moist air to the mass of dry air, ϵ (-) the ratio of moleculair weight of water vapour to dry air, usually assumed as ϵ=0.621 and T_s (K) the absolute soil temperature. The mixing ratio can be obtained as:

$$\tilde{f} = \frac{Rd}{Rv} \frac{e_{act}}{P - e_{act}} \qquad (-) \qquad [35]$$

where Rd = Specific gas constant of dry air ($287\ J.K^{-1}.kg^{-1}$)
Rv = Specific gas constant for water vapour ($461\ J.K^{-1}.kg^{-1}$)
P = Atmospheric pressure (mbar)
e_{act} = Actual vapour pressure (mbar)

where the rightmost denominator accounts for the actual vapour pressure (e_{act}) and the rightmost numerator for the dry air pressure ($P-e_{act}$). The upper limit of the vapour pressure is known as the saturated vapour pressure, which is the vapour pressure just above a plane surface of salt free water. The temperature (°C) dependence of the saturated vapour pressure can be written as:

$$e_{sat} = 1.332\ e^{[(17.25\ T)/(237.3\ +\ T)+1.519]} \qquad (mbar) \qquad [36]$$

The actual vapour pressure can be determined from data of temperature and relative humidity (U): $e_{act} = U\ e_{sat}$. The relative humidity of moist soil air can be derived from the total pressure head (h_{tot}) according eq. [1].
The movement of moist soil air is proportional to the gradients of virtual temperature. Thermal convection occurs when the Rayleigh number of a specific layer at a certain moment is higher than a critical Rayleigh number under the same conditions (e.g. Ribando and Torrance, 1976). Thermal induced convective vapour movement is proportional with the thermal convective velocity (Vca) of moist soil air. Vca can be estimated, comparing the calculated conductive soil heat flow at one hand, and the observed sum of conductive and convective soil heat flow on the other hand (heat balance equation, eq. [15]). This results in the derivation of the apparent soil thermal conductivity (λ_s') as given in the conduction-like heat balance

(eq. [16]). The approximation of $\lambda_s' - \lambda_s^*$ is only a reasonable approximation for small depths (1 cm) with constant heat conductive properties. With larger depths, the soil is not homogeneous so that the difference between the apparent and the "effective" properties may be related with transient properties e.g. water content. Equation 37 is derived from the conduction-like continuity equation (eq. [16]) and the conduction-convection continuity equation (eq. [15]) applying linear temperature gradients across small depths (Menenti, 1984). Similar formula for λ_s' was given by de Marsily (1986) who showed that λ_s' is the sum of λ_s^* and a term due to convective flow.
Taking the limit of Vca=0, i.e. no soil air convection, λ_s' and λ_s^* should be identical.

$$\lambda_s' = \lambda_s^* + \rho_a \, Cp/Vca/\delta z \qquad (W.m^{-1}.K^{-1}) \qquad [37]$$

Similarily as in cases with thermal convective vapour transport, the velocity of diffusive vapour transport can be obtained after the substitution of Vca with Vda.

When the continuous surrounding medium is water i.e. under the evaporation front, conductive heat movement will be the dominant heat transport since vapour flow is eliminated. The "effective" thermal conductivity will then increase with the large thermal conductivity of water. Since the relative humidity and the temperature under the transition zone are more stable, thermal convection is practically ruled out. The velocity of vapour movement in moist soil air can than be expressed as a diffusive flow pattern (Vda).
The difference between λ_s' and λ_s^* will be smoothed out so that errors in the estimation of the vapour flow velocity can be introduced. To face this problem with partly water filled pores, an equation different from eq. [37] valid for a homogeneous thin layer (1 cm) has been applied.

$$\frac{\partial \lambda_s'}{\partial z} = - \rho_a \, Cp \, Vda \qquad (W.m^{2}.K^{-1}) \qquad [38]$$

Figure 6 illustrates the particular procedures to analyse the convective- and difusive flow velocity.

The apparent thermal conducivity in the present report is repeatedly

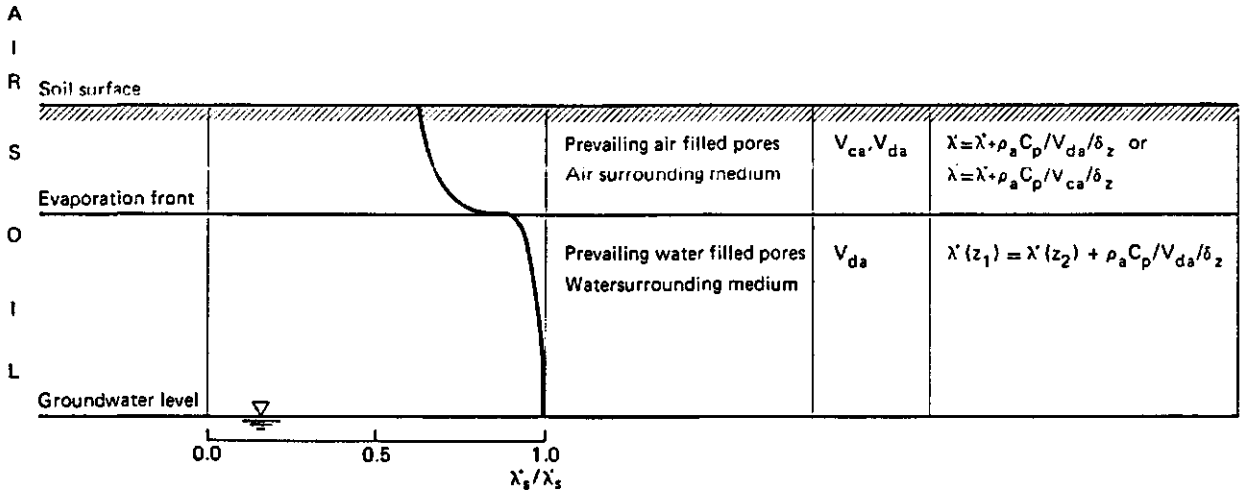

Fig. 6. Schematization of the effective and apparent soil heat conductivity in order to establish the convective- (Vca) and diffusive (Vda) flow velocity of moist soil air

denoted as an important parameter for the calculation of R_{sh} (see e.g. section 3.1.3). Field investigations are mandatory to get appropriate values of λ_s'. Fieldwork carried out in the Western Desert of Egypt confirmed that the soil apparent thermal conductivity is larger than the effective soil thermal conductivity. The peak of the convection process was noticed around 16.00 hour. An alternative procedure to get data on λ_s', is to combine measured values of apparent thermal diffusivity (a') with the theoretical soil heat capacity $(C)_s^*$. For this, the calculation of the effective soil heat capacity $(C)_s^*$ has to be carried out in advance by means of eq. [13].

$$\lambda_s' = a' \ (\rho c)_s^* \qquad (W.m^{-1}.K^{-1}) \qquad [39]$$

The apparent thermal diffusivity can be obtained from observed soil temperature measurements by applying one or more of the following methods:

- La-place transformation
- Green's function
- Ratio of temperature amplitudes

The solution given by the La-place transformation sounds positive, but sets of diurnal measurements recorded with fixed intervals are required, which are seldom available. Disadvantage of the Green's function method is that the soil profile is implicitly assumed to be homogeneous, i.e. constant a-

value. The most practical solution is the method of ratio of temperature amplitudes:

$$a' = \frac{\Omega}{2} z^2/[\text{Ln } A(0) - \text{Ln } A(z)]^2 \qquad (m^2.s^{-1}) \qquad [40]$$

where Ω ($rad.s^{-1}$) is the angular frequency, A(0) the temperature amplitude at surface level and A(z) the soil temperature amplitude at a particular depth. This implies that the thermal diffusivity can be depth dependent, which agrees with varying soil water and vapour content profiles. Combination of Eq. [22] and Eq. [40] yield in eq. [39] which gives the apparent soil thermal conductivity looked for. Hence, the soil resistance factor for heat flow (R_{sh}) can be calculated from the apparent thermal diffusivity. The resistance factor for vapour transport (R_{sv}) will be derived in the next section.

3.2.6. Diffusion of vapour in the moist soil air

It is reminded that the possible free convection and vapour diffusion were anticipated in previous paragraph. Let us assume that the onset of free convection is possible ($q_v = - \rho_v$ Vca). Therefore it was mentioned in the section of heat convection, that thermal convection of soil air can be related to the convective air flow velocity. Yet, the vapour density of this convective movement has to be derived with the perfect gas approach (Boyle-Gay-Lussac) from the virtual temperature in order to predict the vapour flux. This difficulty can be solved by introducing following set of equations:

$$\rho_a = \frac{P}{Rd\ T_{vi}} \qquad (kg.m^{-3}) \qquad [41]$$

$$\rho_v = \rho_a\ r \qquad (kg.m^{-3}) \qquad [42]$$

$$q_v = - \rho_v \text{ Vca} \qquad (kg.m^{-2}.s^{-1}) \qquad [43]$$

where ρ_a = Dry air density ($kg.m^{-3}$)
ρ_v = Vapour density ($kg.m^{-3}$)
r = Mixing ratio (-)
T_{vi} = Virtual temperature (K)

P	= Total gas pressure	($N.m^{-2}$)
Rd	= Specific gas constant for dry air	($287\ J.K^{-1}.kg^{-1}$)
Vca	= Convective flow velocity	($m.s^{-1}$)
q_v	= Vapour flux	($kg.m^{-2}.s^{-1}$)

When convective flow velocity (Vca) between the evaporation front and the surface is known from the apparent soil heat properties, an "effective" vapour diffusivity (D_{eff}) can be derived from Fick's law for the diffusion of water vapour in air (see eq. [10]) since both the vapour flux (q_v) and the vapour density distribution ($\partial\rho_v/\partial z$) is known. This effective diffusivity can be related to the vapour resistance (R_{sv}) required for the combination equation (eq. [6]).

The situation is more complicated with diffusive vapour transport, since plural vapour diffusivities are unknown. Two types of vapour diffusivities have to be distinguished:
- isothermal vapour diffusivity (eq. [44])
- thermal vapour diffusivity (eq. [45])

$$D_{vs,\theta} = D_{vs} \left(\frac{\rho_v\ g}{R\ T} \frac{\partial h_{tot}}{\partial \theta}\right) \qquad (m^2.s^{-1}) \qquad [44]$$

$$D_{vs,T} = D_{vs} \left(U \frac{\partial \rho_v^{sat}}{\partial T_s} + \rho_v^{sat} \frac{\partial U}{\partial T_s}\right) \qquad (m^2.s^{-1}) \qquad [45]$$

The diffusion coefficient of water vapour in soil air (D_{vs}) can be derived when the path length due to pore geometry (tortuosity) and an additional mass flow factor i.e. "enhancement" factor are taken into account (Currie 1960, Feddes 1971) as:

$$D_{vs} = (\xi 0.83\ X_a^{1.7}\ D_{va}) \qquad (cm^2.s^{-1}) \qquad [46]$$

with

$$D_{va} = \frac{23.3}{P} \left(\frac{T}{273}\right)^{2.3} \qquad (cm^2.s^{-1}) \qquad [47]$$

where ξ	= enhancement factor	(-)
X_a	= air filled porosity	($cm^3.cm^{-3}$)
P	= atmospheric pressure	(mbar)
T	= temperature	(K)

The bottle-neck of this approach is the unpredictable value of the enhancement factor (1-100), so that this approach can only be applied after extensive laboratory experiments. The depicted method can be checked against a different approach, but one has to consider the onset of thermal convection as well. It should be realized that the criterion for free convection is somewhat questionable since the actual field conditions cannot be fully idealized. The onset of thermal convection by means of the Rayleigh number then becomes difficult to evaluate. Despite the fact that the above depicted theories supplies the only appropriate physical description, it is stressed here that the apparent soil thermal conduction theory is applied above the evaporation front to obtain the diffusive vapour velocity as well. The same procedure to find an "effective" vapour diffusivity will therefore be followed, considering a diffusive velocity (Vda) instead of a convective velocity (Vca) (see Fig. 6).

The vapour transfer coefficient cannot be computed in cases without gradient of virtual temperature ($\partial Tvi/\partial z=0$). The maximum possible resistance is then arbitrary limited to $R_{sv} = 10^{15}$ s.m^{-1}.

3.2.7. Matric pressure head distribution in the entire soil profile

The problem addressed in this section is that the matric pressure head above the evaporation front has to be associated with a gaseous medium in predominantly air filled pores. Fundamental fluid transport laws like Darcy's law have to be replaced by laws for the gaseous phase. Consequently, the pressure head in a gaseous surrounding medium has to be estimated from the relative humidity of moist soil air in equilibrium with water in the liquid phase by applying Kelvin's law (see eq. [1]).

This means that the derivation of the matric pressure head above the liquid-vapour interface is different from the calculation procedure of matric pressure head below it. Instead of considering the classical Richard's fluid mass equation, a vapour type mass continuity equation has to be applied above the evaporation front. The vapour flux equation is of the Fick's diffusion type.

$$\frac{\partial \rho_v}{\partial t} = - \frac{\partial q_v}{\partial z} \qquad (kg.m^{-3}.s^{-1}) \qquad [48]$$

The above mentioned vapour density of moist soil air plays a significant role in the determination of the total (read: osmotic- and matric) pressure head. The actual vapour pressure, can be simply found from the vapour density by eq. [49]. The solution of an equation accounting on vapour density and vapour pressure yields:

$$e_{act} = (\rho_v \; Rv \; T_s) \qquad (10^{-2} \text{ mbar}) \qquad [49]$$

where Rv (461 $J.K^{-1}.kg^{-1}$) is the specific gas constant for water vapour. In order to express the relative humidity quantitatively, actual vapour pressure as well as saturated vapour pressure have to be known.
The saturated vapour pressure can be obtained through its dependence on temperature (eq. [36]).
A peculiar effect on the gaseous phase in a saline medium has to be noticed. The actual vapour pressure close to a saline medium has to be lowered since the movement of vapour molecules is restricted. Actual vapour pressure then is besides the solid-liquid forces, also affected by the solute concentration of the solvent. Equation [50] describes the lowering of actual vapour pressure above a saline water plane with a varying NaCl solute concentration.
Note that this equation holds also true for the vapour pressure in air. The linear regression coefficients were obtained after a curve fitting procedure with data from Robinson and Stokes (1955).

$$U = e_{act}/e_{sat} = (1 - 0.039 \; C_{na}) \qquad (-) \qquad [50]$$

where C_{na} ($mol.l^{-1}$) is the NaCl solute concentration. The conservation of energy of a fluid particle can be expressed per unit of weight and accounting on osmotic forces according eq. [52]. Having established the total pressure head by means of Kelvin's law, the matric pressure head can be found after substraction of the osmotic pressure head (eq. [53]). One has to note that the molecular weight and density of saline water differ from pure water. The molecular weight may be conceived as the weighted mean value of the molecular weights of water and salt. In case of NaCl salt, the following equation is applicable:

$$\tilde{M} = \frac{\rho_{na}}{\rho_w} 0.0585 + \frac{\rho_{pure}}{\rho_w} 0.018 \qquad (kg.mol^{-1}) \qquad [51]$$

where ρ_w, ρ_{na} and ρ_{pure} are the densities of the total solution, the solutes apart and water respectively. The density of the total solution (ρ_w) ("heavy water") is worked out in section 3.2.8.

$$H = h_m + h_{osm} + h_z \quad \text{and} \quad (m) \qquad [52]$$

$$h_{tot} = h_m + h_{osm} \quad (m) \qquad [53]$$

where H = hydraulic head (m)
h_m = matric pressure head (m)
h_{osm} = osmotic pressure head (m)
h_z = elevation head (m)
h_{tot} = total pressure head (m)

The osmotic pressure head is linear related with the solute concentration according the state of a perfect gas. Van 't Hoff's equation can be written in unit of weight:

$$/h_{osm}/ = \frac{Ru\ T_s\ C}{g\ \rho_w}\ d \quad (10^3\ m) \qquad [54]$$

where C is the concentration ($mol.l^{-1}$), Ru (8.314 $J.mol^{-1}.K^{-1}$) the universal gas constant, T_s (K) the absolute soil temperature and d (-) v. 't Hoff's disscociation factor. Latter parameter is the increment of dissolved moles by dissociation of electrolyte molecules. NaCl is an example of a completely dissociating salt because both iones contribute to the dissociating process. Combination in sequential order of eq. [50], eq. [51], eq. [1], eq. [53] and eq. [54] shows values of v. 't Hoff's dissociation factor in a NaCl solution around d=1.8. This agrees nicely with values published by Barrow (1966).
Gradient of pressure head causes water to move. The gradient of osmotic pressure head is difficult to estimate since h_{osm} varies with the (transient) solute distribution. This facet can only be solved when solute transport is mathematically coupled with unsaturated soil water flow e.g. SWASALT-model (Kabat et al., 1988b). Osmotic forces are quite evident in rainless desert soils with a shallow groundwater table. We will provisionally assume that the ratio of the total pressure head ($\partial h_{tot}/\partial z$) over the ratio of the matric pressure head ($\partial h_m/\partial z$) equals the ratio

AIR

Soil surface

SOIL

Diffusive and convective vapour transport Evaporation front	$D_{v,eff.}$	$\frac{\partial \rho_v}{\partial t} = -\frac{\partial q_v}{\partial z}$	$q_v = -D_{v,eff.} \frac{\partial \rho_v}{\partial z}$	$\frac{\partial \rho_v}{\partial t} = \frac{\partial}{\partial z}(D_{v,eff.} \frac{\partial \rho_v}{\partial z})$	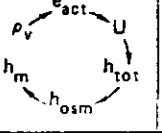	$\rho_v(z) - h_m(z)$
Liquid transport Groundwater level	$K(h_m)$	$\frac{\partial \theta}{\partial t} = -\frac{\partial q_l}{\partial z}$	$q_l = -K(h_m)(\frac{\partial h_m}{\partial z} + 1)$	$\frac{\partial h_m}{\partial t} = \frac{1}{C(h_m)} \frac{\partial}{\partial z}[K(h_m)(\frac{\partial h_m}{\partial z} + 1)]$	No conversion	$h_m(z)$
Type of transport	Transport parameter	Continuity equations	Kinetics of flow	Combination equation	Conversion equations	Matric pressure head distribution

Fig. 7. Establishment of the pressure head distribution ($h_m(z)$) according the different continuity equations of water in the vapour and liquid phase respectively above and below the evaporation front

$K(h_m)/K(h_{tot})$ (see BASTIAANSSEN and HALBERTSMA, 1989). An additional study towards this subject has to be carried out. Hence, the Darcy equation is written in the "classical form" (eq. [3]). The preceding theories are schematized into Fig. 7.

3.2.8. Correction for the bulk properties of soil water

The unsaturated hydraulic conductivity ($K(h_m)$) and the water retention characteristic ($h_m(\theta)$) play a key role in the liquid transport capacity through partly gas filled pores. The importance of these hydraulic properties may require an extensive approach because interactions between soil fluid (liquid and vapour) and soil solid (grains and pore walls) phases do also depend on temperature and salt concentration as well. It should be understood that large temperature oscillations and large solute concentrations may modify the bulk properties of liquid water. To obtain corrections for this phenomenon, very complicated experiments are required. Theoretical corrections for the bulk properties of water can be calculated considering the partial derivatives of the matric pressure head with respect to temperature ($\partial h_m/\partial T_s$) and salt concentration ($\partial h_m/\partial C$).

Identically, the partial derivatives of the unsaturated hydraulic conductivity with respect to temperature ($\partial K(h_m)/\partial T_s$) and salt concentration ($\partial K(h_m)/\partial C$) can be derived.

First the contribution of the bulk properties of water have to be discussed:

ρ_w = density of water in the liquid phase ($kg.m^{-3}$)

η_w = dynamic viscosity ($N.s.m^{-2}$)

σ_{wa} = surface tension of water against air ($N.m^{-1}$)

The variation of the temperature related density of water in the liquid phase can be found from tables such as table F-5 in the Handbook of Chemistry and Physics. Table F-30 of the same book deals with temperature related surface tension of water against air while table F-36 contains the temperature related viscosity (see Fig. 8). As a reference, values are illustrated in appendix 5. Statistical relations are derived to relate viscosity ($N.s.m^{-2}$) with temperature (°C) and yield (also table F-36):

when T_s < 20 °C, C=0 $mol.l^{-1}$

$$\log(\eta_w) = [1301/(998.3+8.18(T_s-20)+0.0059(T_s-20)2)]-3.3 \quad (10^{-4}\ N.s.m^{-2}) \quad [55]$$

when T_s > 20 °C, C=0 $mol.l^{-1}$

$$\log(\eta_w/1.002) = [1.327(20-T_s)-0.001(T_s-20)2]/(T_s+105) \quad (10^{-4}\ N.s.m^{-2}) \quad [56]$$

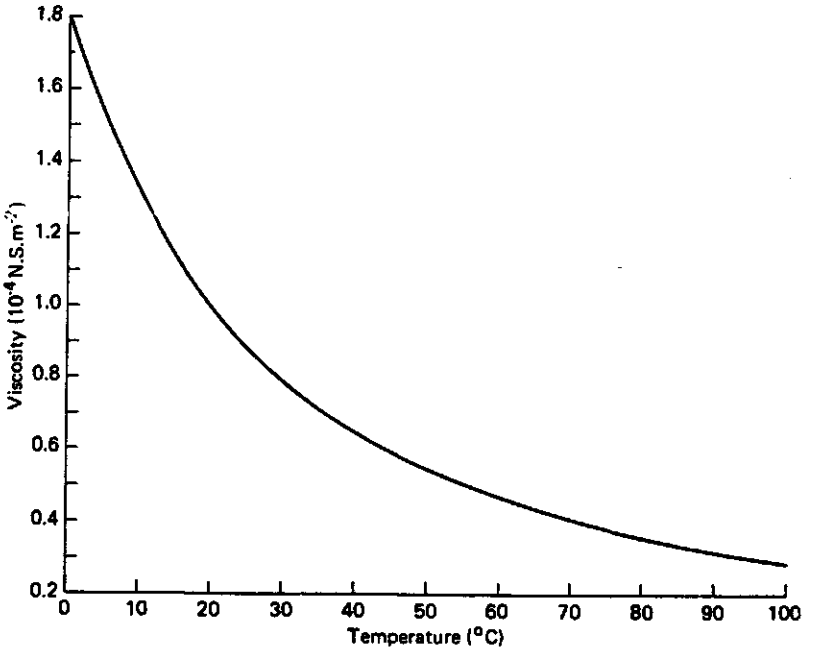

Fig. 8. Relationship between temperature and viscosity of water

The modifications of bulk properties caused by the presence of salt solutes are all best fit approximations derived from data sets found in the same handbook.

for T_s = 20 °C:

$$\rho_w(C) = 998.23 + (C\ 37.5) \qquad \text{(table D-261)} \qquad (kg.m^{-3}) \qquad [57]$$

$$\eta_w(C) = e^{(0.10\ C\ -\ 0.064)} \qquad \text{(table D-261)} \qquad (10^{-4}\ N.s.m^{-2}) \qquad [58]$$

$$\sigma_{wa}(C) = 72.75 + C\ 1.924 \qquad \text{(table F-28)} \qquad (10^{-3} N.m^{-1}) \qquad [59]$$

Having defined the bulk properties of water, the partial derivatives of these properties with respect to temperature and salt concentration can be calculated.

It appears that all derivatives with respect to temperature are negative, while for salt effects the opposite is evident.

The matric pressure head is a function of ρ_w and σ_{wa}, while the saturated hydraulic conductivity (K_{sat}, $m.s^{-1}$) dependens on ρ_w and η_w among others. The unsaturated hydraulic conductivity ($K(h_m)$, $m.s^{-1}$) is a combination of both h_m and K_{sat} so that all properties i.e. ρ_w, η_w and σ_{wa} has to be involved. Accordingly, the matric pressure head can be calculated analogue to eq. [5] as:

$$h_m = \frac{1}{\rho_w\ g}\ \frac{2\ \sigma_{wa}}{r_m} \qquad (m) \qquad [60]$$

Where r_m (m) is the effective radius of curvature of the air filled pores. A standard approach to describe $K(h_m)$ is the partition with the saturated hydraulic conductivity:

$$K(h_m) = b(h_m)\ K_{sat} \quad \text{with} \qquad (m.s^{-1}) \qquad [61]$$

$$K_{sat} = \rho_w\ g\ K/\eta_w \qquad (m.s^{-1}) \qquad [62]$$

Where $b(h_m)$ (-) is the relative hydraulic conductivity and K (m^2) the spe-

cific permeability. The variation of h_m and K_{sat} with respect to environmental conditions can now be derived (see table 5). The relevance of the change in the hydraulic properties is more evident when one has either to deal with high temperature or high salt concentration only. The combined effect compensates large changes of the bulk properties of water.

Table 5. Partial derivatives of bulk properties of water with respect to temperature and salt concentration

hydraulic parameter	temperature	solute concentration
h_m	$\frac{\partial}{\partial T_s}(\sigma_{wa}/\rho_w) < 0$	$\frac{\partial}{\partial C}(\sigma_{wa}/\rho_w) > 0$
K_{sat}	$\frac{\partial}{\partial T_s}(\rho_w/\eta_w) < 0$	$\frac{\partial}{\partial C}(\rho_w/\eta_w) > 0$

The partial derivatives of $h_m(\theta)$ and $K(h_m)$ can be given now. The partial derivatives with respect to salt concentration are analogue with the partial derivatives with respect to temperature (Appendix 6). Here only one set is described.

$$\frac{\partial h_m}{\partial T_s} = \frac{\rho_w h_m}{\sigma_{wa}} \frac{\partial}{\partial T_s}\left(\frac{\sigma_{wa}}{\rho_w}\right) \qquad (m.K^{-1}) \qquad [63]$$

$$\frac{\partial K(h_m)}{\partial T_s} = \frac{\rho_w g k}{\eta_w} \frac{\partial b(h_m)}{\partial h_m} \frac{\partial h_m}{\partial T_s} + g K b(h_m) \frac{\partial}{\partial T_s}\left(\frac{\rho_w}{\eta_w}\right) \quad (m.s^{-1}.K^{-1}) \qquad [64]$$

These theories are implemented in the EVADES-model by the adaption of the matric pressure head and unsaturated hydraulic conductivity through the temperature increment between the laboratory (T_{lab})- and the field (T_s) situation:

$$h_m(\theta) = h_m(\theta) + \frac{\partial h_m}{\partial T_s}(T_s - T_{lab}) \qquad (m) \qquad [65]$$

$$K(h_m) = K(h_m) + \frac{\partial K(h_m)}{\partial T_s}(T_s - T_{lab}) \qquad (m.s^{-1}) \qquad [66]$$

4. STRUCTURE OF THE EVADES-MODEL

4.1. BOUNDARY CONDITIONS

The matric pressure head at the groundwater table (h_m=0) is the lower boundary condition of the soil system in the EVADES-model (prescribed pressure head). Alternatives of the boundary conditions at the bottom of the system, such as applied in the SWATRE-model, has not yet been implemented in the current version of the EVADES-model. The depth of the groundwater table can be either taken constant or as a daily variable. For bare soils, the potential evaporation flux according to v. Bavel (1966) is the maximum possible flux through the surface. Hence, the vapour flux can never exceed the potential evaporation rate. The minimum possible matric pressure head at the surface is governed by eq. [1] and the salt concentration at the surface (eq.[53]) as well.

4.2. GEOMETRY OF THE COMPARTMENT NETWORK

The soil system is divided into a grid of soil compartments of unequal size with a depth-time domain (see Fig. 9). The nodal points are located at the centre of the compartments. The total number of compartments is fixed at 40. The upper 20 compartments have a fixed 1 cm thickness. Thus micro-scale flow domain provides for detailed temperature distribution and stabilization of the position of the evaporation front. An improved description of the interface displacement and soil temperature regime, results in a better estimation of the soil resistance factors for the transport of vapour and heat. Hence, maximally 20 compartments are left between 20 cm below surface level and the bottom of the soil system. It is recommendable to select the size of the variable compartment thickness below the 20 cm layer, not thicker than 10 centimeter. The latter means that the total flow domain has a maximum depth of 220 cm. Yet, situations with a deep groundwater table such as in cases with free drainage, cannot be simulated with the present stage of the model.

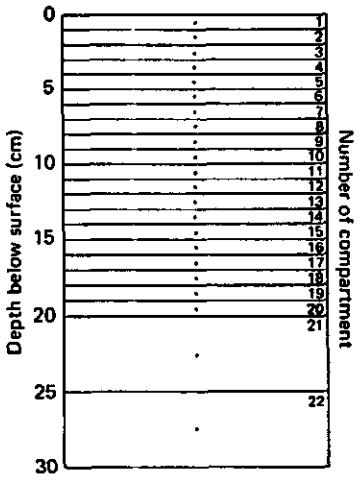

Fig. 9. Compartment scheme of the verticale profile; the variable compartment thickness is indicated

The nodal points of the finite difference scheme are located at the centre of each compartment. Maximum 5 different layers with different physical properties can be determined. The boundary of each layer should be exactly located at the edge of a compartment i.e. in the midle of two nodalpoints.

4.3. NUMERICAL SOLUTION SCHEME

Combination of the equations for mass conservation and transport results in second order partial differential transport equations which have to be solved numerically. Two types of fluid transport have to be distinguished; the liquid mass continuity equation applies below the evaporation front $\partial\theta/\partial t = -\partial q_l/\partial z$ where q_l ($cm.d^{-1}$) is the Darcy-type liquid flux while a vapour mass continuity equation has to be applied above the evaporation front $\partial\rho_v/\partial t = -\partial q_v/\partial z$ with q_v ($kg.m^{-2}.s^{-1}$) the Fick-type vapour flux. To evade the difficulties of the transition from vapour diffusion in air to vapour diffusion in soil, the diffusion coefficient is written is an "effective" diffusion coefficient.

$$\frac{\partial \rho_v}{\partial t} = \frac{\partial}{\partial z}\left(D_{eff}\frac{\partial \rho_v}{\partial z}\right) \qquad (kg.m^{-3}.s^{-1}) \qquad [67]$$

The implicit partial differential equations have to be rearranged using explicit linearization of matric pressure head and vapour density gradients. When the boundary and initial conditions e.g. matric pressure head in an equilibrium profile with the groundwater table, are known, the system

of linear equations can be solved. The numerical approximation of eq. [68] is made analogue with the finite difference technique to solve the Richard's equation. A linear expression for the vapour content at each intermediate nodal point is found by meas of the Thomas algorithm technique (Remson, 1971).

$$\rho_{v_j}^{i+1} = -A_j \rho_{v_{j+1}}^{i+1} + B_j \rho_{v_j}^{i+1} - D_j \rho_{v_{j-1}}^{i+1} \quad (kg.m-3) \qquad [68]$$

where j is the depth-index and i is the time-index with u and l being the vertical distance with the upper and lower nodal point respectively. (for more details see appendix 7). For a detailed description of the finite difference solution of the Richard's equation, one is refered to HAVERKAMP et al. (1977) and KABAT et al. (1989).

The difficulty with this type of coupled liquid-vapour flow is that the depth of the evaporation front has to be known a priori. Remember that this interface is the boundary between the vapour and liquid system. The applied procedure is that in first step liquid flow is assumed across the entire profile. The matric pressure head distribution according the solution given by the Richard's equation is established first. The numerical solution procedure starts from the upper boundary of the compartment network.

The depth of the evaporation front can be found from the criterion that the pressure head below the evaporation front is, absolutely seen, smaller than the pressure head at the evaporation front (hme). The evaluation of this criterion starts from the groundwater table upwards at each time step. At each nodal point, hme is calculated first from the soil temperature. Then, hme is compared with hm-value obtained from the Richard's equation at the same time step. If /hm/ is smaller than /hme/, the above laying compartment will be considered. This procedure will be repeated until /hm/ is larger than /hme/.

A logarithmic interpretaton between the nodal points in which the evaporation front is situated will be done to establish the exact depht of the front.

After determination of the location of the evaporation front, all compartments between the surface and the evaporation front will be recalculated with the Fick-type vapour continuity equation. The matric pressure head distribution ($h_m(z)$) above the evaporation front can finally be obtained from the vapour density distribution ($\rho_v(z)$). The required theories for this convertance were exposed in section 3.2.7. and Fig. 7.

The allowed time step is evaluated by either a prescribed maximum change of soil water content or an assigned value of the maximum change of vapour content:

$$\Delta t = \frac{\Delta\theta_{max}}{(\Delta\theta/\Delta t)_{max}} \quad \text{or} \quad \Delta t = \frac{\Delta\rho_{v\ max}}{(\Delta\rho_v/\Delta t)_{max}} \qquad (d) \qquad [69]$$

where θ_{max} is a prescribed value, valid for the compartments underlying the evaporation front. Consequently, $\rho_{v\ max}$ will be applied for the compartments above the evaporation front. The ratio $(\Delta\theta/\Delta t)_{max}$ or $(\Delta\rho v/\Delta t)_{max}$ is the maximum calculated change of water content or change of vapour density over all compartments at time i respectively. The simulation process is continued by the evaluation of the matric pressure head distribution at the next time step.

4.4. INPUT PARAMETERS

The required input data contains meteorological and soil physical variables. All input parameters as listed in table 6 have to be prescribed in the central input file "EVADES.IN".

It goes without saying that on site observations are required to get proper input data. Such a comprehensive dataset is however difficult to observe in the field. Even, some vertical profiles of parameters are required.
At least, air temperature, soil temperature, surface temperature, relative humidity, windspeed, incident and reflected irradiance, estimated uniform solute concentration, depth of the groundwater table, the $K(h_m)$ and $h_m(\theta)$ relationship and the water content profile $z(\theta)$ have to be recorded.

The value of the remaining not observed parameters can be assessed by means of alternative techniques. Diffuse irradiance can be estimated on basis of cloudiness, recorded at meteorological stations. The bulk density can be computed from the weighted mean volumetric fraction of porosity, quartz and

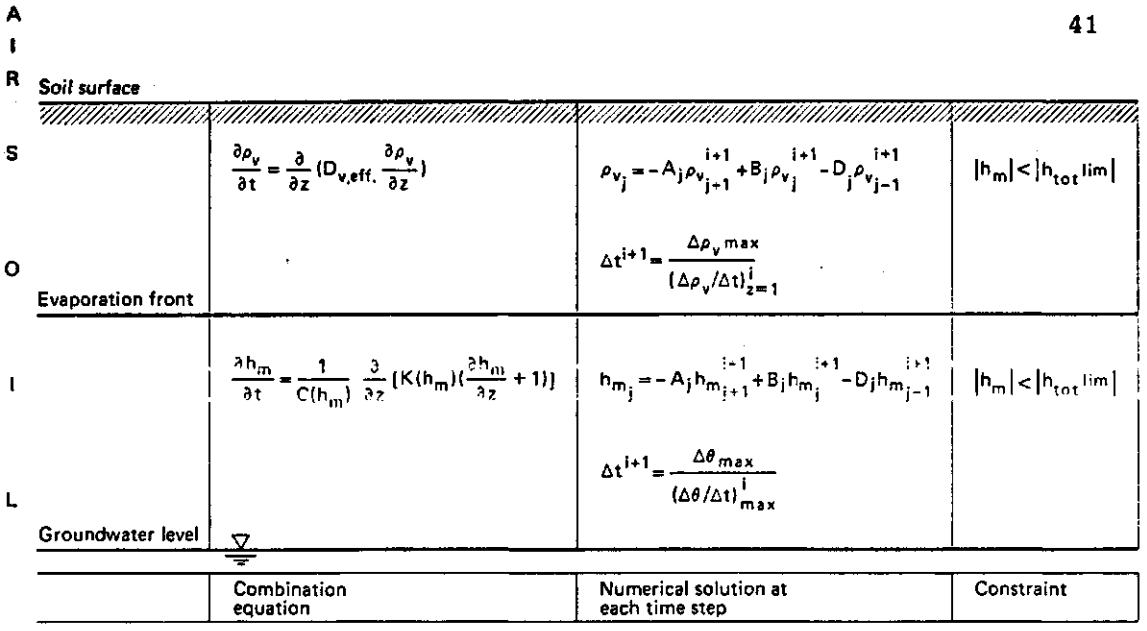

Fig. 10. Schematic overview to find the matric pressure head in the entire soil profile

Table 6A. Overview required input parameters for the EVADES-model; part A, Meteorological conditions

Parameter	Number of layers	Unit	Purpose	Energy process	eq.
Air	⩾ 2	°C	Vapour pressure deficit	Latent heat flux	6,76
temperature	⩾ 2	°C	Sensible heat flux	Sensible heat fl.	70
	1	K	Longwave sky radiation	Net radiation	77
	⩾ 2	K	Richardson number	Sensible,latent heat flux	90
Relative	⩾ 1	-	Vapour pressure deficit	Latent heat flux	6,76
humidity	1	-	Pressure head surface level	Darcy flux	3
Windspeed	⩾ 2	$m.s^{-1}$	Aerodynamic resistance	Sensible,latent heat flux	92,93
	⩾ 2	$m.s^{-1}$	Richardson number	Sensible,latent heat flux	90
Inc. irrad.	-	$W.m^{-2}$	Net shortwave radiation	Net radiation	77
Diff. irrad.	-	$W.m^{-2}$	Surface reflectance	Net radiation	77
Zenith angle	-	-	Surface reflectance	Net radiation	77
Time of sunset,sunrise	-	hour	Day/night time windspeed	Sensible,latent heat flux	90
	-	hour	Relative humidity	Latent heat flux	6,76
	-	hour	Apparent emissivity	Net radiation	79

Table 6B. Overview required input parameters for the EVADES-model; part B, Soil conditions

Parameter	Number of layers	Unit	Purpose	Energy process	eq.
Surface	1	K	Net longwave radiation	Net radiation	77
temperature	1	°C	Soil heat flux	Soil heat flux	19
	1	°C	Apparent thermal diffusivity	Convective heat flux	40
	1	K	Pressure head surface level	Darcy flux	3
Soil	⩾ 5	°C	Soil heat flux	Soil heat flux	19
temperature	⩾ 5	°C	Apparent thermal diffusivity	Convective heat flux	40
	⩾ 5	K	Soil air humidity	Convective heat flux	34
	⩾ 5	°C	Correction soil bulk properties	Darcy flux	65,66
Norm. reflect.	-	-	Surface reflectance	Net radiation	77,78
Depth ground water tabel	1	cm	Bottom boundary unsaturated zone	Darcy flux	3
Solute conc.	⩾ 5	$mol.l^{-1}$	Correction soil bulk properties	Darcy flux	102,103
	⩾ 5	$mol.l^{-1}$	Lowering vapour pressure	Latent heat flux, Convective heat flux	6,76 50
Vol. water cont. profile	⩾ 5	$cm^3.cm^{-3}$	Model calibration	Fluid flux	-
Bulk dens.	⩾ 2	$kg.m^{-3}$	Heat storage	Soil heat flux	20
Salt conc.	⩾ 5	$cm^3.cm^{-3}$	Thermal properties	Soil heat flux	22,31
Sat. conduc.	1	$cm.d^{-1}$	Relative unsat. hydr. cond.	Darcy flux	61
hm(θ)-curve	1	-	$h_m(\theta)$ relationship	Darcy flux	3
$K(h_m)$-curve	1	-	$K(h_m)$ relationship	Darcy flux	3

salt minerals. The porosity and saturated conductivity can be obtained via the retention and conductive characteristics, eventually described by the parameter estimation technique (KABAT et al, 1988c). The diurnal sun zenith angle cyclus and extra-terrestrial sunshine duration can be found in tables (Smithsonian Meteorological Tables, 1969).

4.5. OUTPUT PARAMETERS

The EVADES-model foresees in several intermediate calculation results, which fit the users goal to follow the total physical transport process quantitatively. Not only the final evaporation rate, but also intermediate steps can be of outstanding interest. Especially the simulated trends among parameters can be very usefull to understand their meaning in the entangled flow process. Eventually, such trends can be applied as input data for simplified fluid transport models e.g. $z_e = f(k(h_m))$. Hence, the heat flow process and the water displacement can be traced in detail. Intermediate output results are presented in twelve different output files. Table 7 gives an overview of all output information at each stage of the computation scheme.

Table 7. Output files of the EVADES-model

Filename	Output parameter
EVADES.EX	z_e, LE_{pot}, LE_{act}, FLXS(1), R_{sv}, R_{sh}, $h_m(z_e)$, h_m
EVADES.ACT	ρ_a, VPD, S_a, S_s, R_{av}, R_{ah}, Ri, R_n, W_e, G_e, R_{sh}, γ, R_{sv}, LE, $T_a(1)$, U
EVADES.POT	S_a, R_n, G_0, ρ_a, VPD, R_{av}, R_{ah}, U*, Ri, γ, LE, $T_a(1)$, U
EVADES.RES	E_{pot}, E_{pot}(cum), E_{act}, E_{act}(cum), z_e, $\theta(1)$, LE, R_{sw}, $T_a(1)$, $T_s(0)$, R_{ah}, G_e
EVADES.TEM	$T_s(0)$, $T_s(1)$, $T_s(2)$, $T_s(3)$, $T_s(4)$, $T_s(5)$, $T_a(1)$, $T_a(2)$, a'(1), a'(5), a'(10)
EVADES.VAP1	λ_s*, λ_s', a'(1), Vca, e_{sat}, e_{act}, f, T_s, Tvi, ρ_a, ρ_v, q_v
EVADES.VAP2	$\rho_v(0)$, $\rho_v(z_e)$, q_v, D_v, z_e, $\lambda_s'(0)$, $\lambda_s'(z_e)$, T_e, T_0
EVADES.PRH	$h_m(0)$, $U(z_e)$, $h_m(1)$, $h_m(5)$, $h_m(10)$, $h_m(15)$, $h_m(20)$, $h_m(22)$, $h_m(25)$
EVADES.HED	h_{me}, ad h_{me}, θ_e, $k(h_m)(z_e)$, ad $k(h_m)(z_e)$, $\rho T_s/\rho T_s$lab, $\sigma T_s/\sigma T_s$lab, $\eta T_s/\eta T_s$lab, $\rho C/\rho C_{lab}$, $\sigma C/\sigma C_{lab}$, $\eta C/\eta C_{lab}$
EVADES.FLX	R_n, G_0, LE, H
EVADES.STA	Ri, ϕ_v, ϕ_h, u^*_v, u^*_h, $T_a(1)$, $T_a(2)$, dT_a, u(z1), u(z2), z1, z2
EVADES.OUT	General output information

5. FORTRAN CODE

5.1. SUBROUTINES

The model is split up in subroutines with specific procedures. By this approach, the software can be read more easily and becomes more attractive to adapt. Totally 17 subroutines have been implemented. Table 8 gives a list of subroutines and a short explanation of its function.

Table 8. Subroutines of the EVADES-model

Subroutine	Job
RDATA	Reading of the general input data, calculation of equilibrium conditions
PARSOL	Reading and calculation of the soil properties
BOCOBO	Reading bottom boundary conditions
BOCOTO	Reading meteorological data, synchronisation calculations
POTVAL	Calculation of hourly potential latent heat flux values
WATCON	Calculation of soil water content profile
ADAPT	Adaption of the simulated matric pressure head into a matric pressure head with pure water at 20 °C
MOSCON	Calculation of conductivity and differential moisture capacity
VISCO	Calculation of viscosity
FLUXES	Calculation of the Darcy fluxes between the nodes
BOCO	Calculation of boundary conditions
VAPOUR	Calculation of the location of the evaporation front
FRONT	Calculation of the actual evaporation rate
INTGRL	Calculation of cumulative values
DELTIM	Calculation of next time step
HEDCAL	Calculation of the vertical pressure head distribution
OUTPUT	Write data to EVADES.OUT

The double precision Fortan 77 version of the EVADES-model is implemented, compiled and linked on a micro VAX with the VAX/VMS V4.5 operation system. Variable transfer between the separate subroutines is performed with aid of the "include" statement. The file COMMON.FOR acts as the "include" file, where only common blocks are present. During the compilaton procedure, the files EVADES.FOR and COMMON.FOR are engaged together obtaining the EVADES.OBj version. After the linkage procedure, the model will be execuble by means of the EVADES.EXE version. Hence, simulation work can be done when the following scheme is applied:

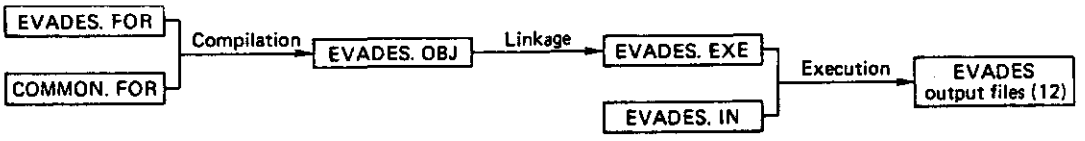

Fig. 11. Overview EVADES-programs

5.2. COMPUTATION SCHEME

The steps of the simulation process can be outlined by mentioning the different subroutines in their order of computation. The main job of each routine is depicted in section 5.1. The theoretical description of each job is presented in chapter 3.

The computation process can be discriminated in a preprocessing and a simulation part. With preprocessing is ment the reading of the input data i.e. input parameters presented in EVADES.IN and calculation of the potential evaporation on hourly basis. The simulation process afterwards uses the boundary and initial conditions as derived from the former step.
Translating this outline in terms of subroutines, the following scheme applies:

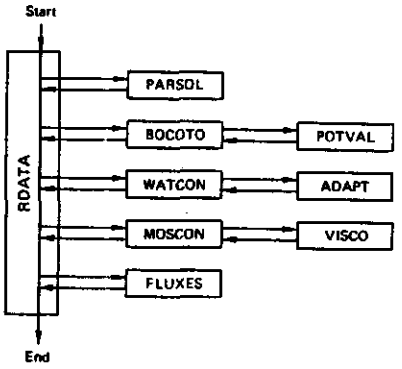

Fig. 12A. Computation scheme in terms of subroutines; reading and calculation of boundary and initial conditions

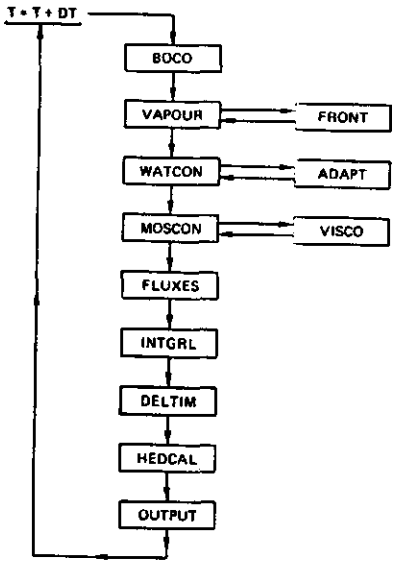

Fig. 12B. Computation scheme in terms of subroutines; simulation actual rate of water flow

6. ANALYSIS OF RESULTS

6.1. VALIDATION

Several simulations were performed to test the new EVADES-model. The model was applied with data collected during fieldwork carried out in the Qattara depression. This field measurements included all the required parameters as listed in table 6. Besides, the actual evaporation was measured by means of the Bowen-ratio energy balance method. Since several sites with different depths of the groundwater table were throughly analysed, it was possible to obtain evaporation measurements under very different conditions. The groundwater table varied between 25 and 68 cm minus surface level.

The principal issue is the simulation of the depth of the evaporation front in combination with the derivation of the soil resistances of vapour and heat flow. As already depicted in Fig. 2, this is strongly related to the soil hydraulic properties. Preliminary hydraulic soil classification was used for the simulations. The classification is based upon measurements of several $h_m(\theta)$- and $K(h_m)$ relationships, which were grouped by means of a clusteranalysis technique of their individual trends, analytically fitted by the v. Genuchten parameters (Bastiaanssen and de Groot,1989).

The simulation results can be verified against measurements of e.g. the soil temperature profile, the soil water content profile and the actual evaporation. The agreement between simulated and observed evaporation rates was quite good, so, the description of the entangled physical processes for bare soil evaporation as included in this model, seems rather accurate. The soil temperature profile can be compared with measured data of a whole diurnal soil temperature cycle. The soil temperature profile was calculated rather well as shown in Fig. 14.

More complicated was the validation on basis of the soil water content profile. The soil water content depends on the soil hydraulic properties.

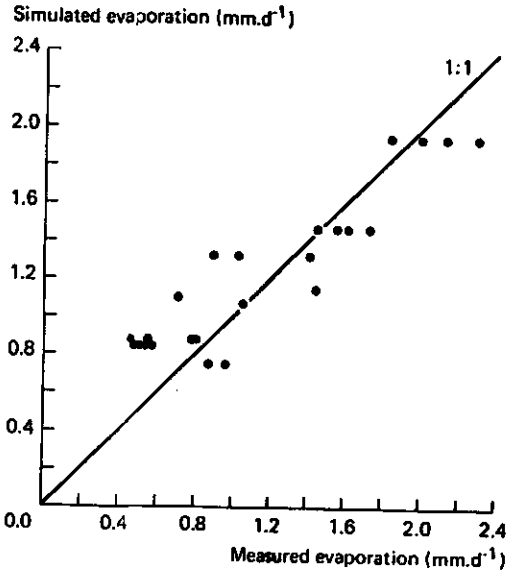

Fig. 13. Measured evaporation according the Bowen-ratio energy balance method versus the simulated evaporation by means of the EVADES-model.
Different depths of the water table at different sites are considered

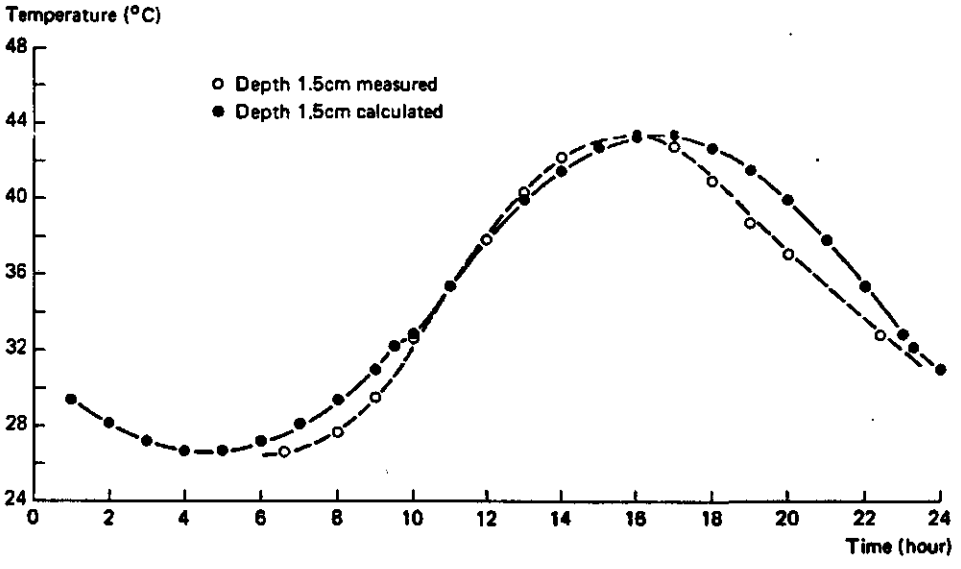

Fig. 14. Measured- and calculated soil temperature profile (1.5 cm) on 12/13 June 1988. A sandy puffy soil situated at Bir Qifar in the Qattara depression is considered

Since the individual $h_m(\theta)$- and $K(h_m)$ relationships, as analyzed at the laboratory, were grouped, the simulation were performed with mean characteristics per group. Consequently, the water content profile for a single spot cannot per definition be identical with the simulation results. However, the variation of hydraulic characteristics in the group of coarse sands was acceptably small so that the model gives accurate vertical profiles of soil water content. The soil water content at the liquid-vapour interface, however, was not accurately simulated since this theoretically defined interface should be conceived as a transition zone were the differential soil water capacity ($\partial\theta/\partial hm$) is not so steep as the model assumes.

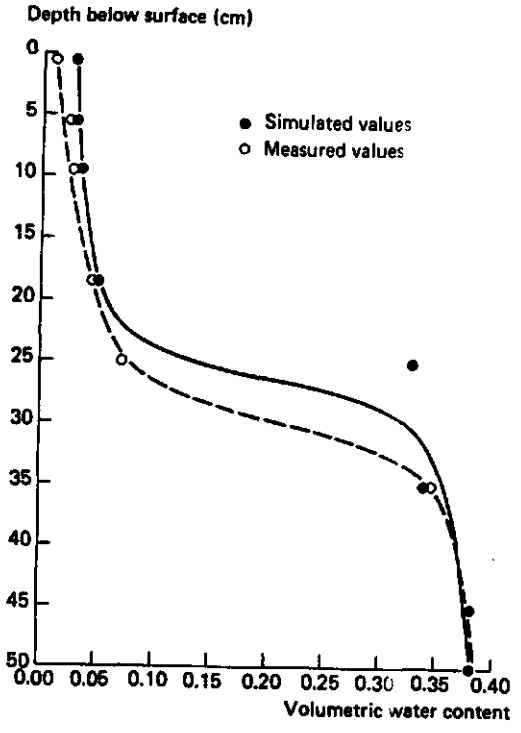

Fig. 15. Measured versus simulated soil water content profiles with the EVADES-model for a bare coarse sand soil as present at Bir Tarfawi in the Soutwestern part of Egypt.

6.2. SHORTCOMINGS AND PROSPECTIVES

Simulation of transient waterflow in unsaturated soils by the EVADES-model is a rather good estimation of the actual evaporation from bare soils.

However a model is a chain of physical laws and is only beneficial when environmental processes can be parameterized. It can be easily understood that surface topography with micro-relief cannot be modelled. Cracks in the saltcrust upto a depth of 30 cm were noted by various authors (Ritchie and Adams, 1974; Menenti, 1984). The vapour flow from such cracks appears to be two orders of magnitude larger than for ordinary diffusion flow rates. This feature requires for an explicit description of soil air convection. Although the latter phenomenon can be modelled for clayey soils (Bronswijk, 1988) the describing functions are not implemented in the EVADES-model.

The concentration of precipitated salts in the top layer varies with depth. Even at larger depths, thick salt layers can be noticed.
Accordingly, the aqueous solution along the profile is variable. The gradient of this solution can be assessed by the analyses of solute concentration from the lower part of the zone. A more relevant but expensive technique is the application of micro-psychrometers which measure the total potential until 80 bar (Gaudu, 1988). If the solute gradient along the whole profile can be determined and simulated, a step forward regarding the gradient of osmotic potential and the correction for the bulk properties of liquid water can be done. Knowing the gradient of osmotic potential, the Darcy equation can be extended with an additive driving force ($\partial h_{osm}/\partial z$). This point of discussion can be realized in the EVADES-model, when a solute transport model is developed (e.g. SWASALT-model).

The presence of dew in the early morning and precipitation is another point of discussion. The microscopic thin dew layer will evaporate during the morning, which in fact can be stated as a second evaporation front overlying the first and main evaporation front. Intermittent precipitation implies the onset of multiple evaporation fronts also, which are not modelled at present. Multiple evaporation fronts should be implemented in the model in a later phase.

Another fact to be mentioned is that dry saline soils are mainly non-vegetated. Transpiration processes are not considered in the present stage of the model. In order to apply the present model for agricultural purposes, e.g. transpiration and crop yield forecasting, a term for the water uptake by roots has to be added such as in eq. [3].

Although the soil water extraction pattern by plants growing under arid conditions are unknown, an attempt to solve this topic has to be made.

A method has been developed to compute the soil temperatures when the depth dependent temperature amplitude (A(z)) and average daily temperature (T(z)) are known. This is a drawback for situations when soil temperature profiles are not measured at regularly intervals. It should be realized that the varying damping depth approach may be an improvement for the present model to forecast soil temperature fields when data is not available. Empirical expressions of the depth dependent thermal diffusivity has to be developed and implemented.

The exact value of the matric pressure head and the unsaturated hydraulic conductivity at each time step are computed by linear interpolations of the $h_m(\theta)$ and $K(h_m)$ relationships. It is preferred to use an analytical function e.g. van Genuchten (1980) or polynomial regression function since it gives a direct expression between θ and K versus h_m. This option in not yet foreseen in the EVADES-model. It also improves the conveniency of the preparation of the input data.

The mathematical solution of the implicit partial differential equation must include an appropriate description of the boundary and intial conditions. Besides the depth of the groundwater table, alternative specifications for the bottom boundary condtition has to built in the future version of the model.

7. SUMMARY

The SWATRE-model is a commonly used and continuous up-dated simulation model, describing water transport in the liquid phase through the porous soil under humid conditions. However, for non-vegetated rainless areas like the Saharian belt, water vapour transport through the extremely dry topsoil forms the limiting factor for capillary rise from the groundwater table.

A new simulation model of bare soil EVAporation in DESerts (EVADES) has been developed to describe vapour displacement in the top soil. The EVADES-model is a combination of the Dirichlet type boundary condition with the soil water displacement described by a Darcy-type equation for liquid transport and a Fick-type equation for movement of vapour. Water evaporate inside the soil at the location where mainly liquid displacement changes into mainly vapour displacement. This layer is the liquid-vapour interface or so called evaporation front. Gas kinetics underlying this theory has been briefly summarized. The evaporation front is defined as the depth where the matric pressure head at the evaporation front coincides with the equivalent matric pressure head obtained by taking the pore radius equal to the mean free path of water vapour.

Potential evaporation is defined as the evaporation rate where the evaporation front is situated at surface level. The lower the evaporation front, the lower the actual evaporation which can be algebraically expressed by considering soil resistance factors to account for flow limiting transport of vapour and heat from the evaporation front towards surface level. These factors can only be derived if the conductive and convective heat flow are precisely described by effective and apparent soil thermal conductivity. Soil heat processes have therefore to be determined in detail. This appears only succesfull if accurate field observations of the temperature distribution inside the heterogenous soil are available.

To increase the accuracy of the determination of the evaporation front, a network of one centimeter compartments in the topsoil (20 cm) is applied.

Either the liquid continuity or the vapour continuity equation applies, depending on the phase. The simulation can be performed in small time increments (less than 30 minutes) because the upper forcing factor (potential evaporation) is calculated as hourly values.

The validation of the EVADES-model has been performed with meteorological and hydrological data collected in the Western Desert of Egypt. The results were calibrated against observed evaporation fluxes, soil temperature profiles and soil water content profiles. Although the field conditions were quite different between the sites (variable evaporation front), the agreement between the measured and simulated data was quite good.

REFERENCES

BARROW, G.M., 1966. Physical chemistry. Second edition. p. 843.

BASTIAANSSEN, W.G.M., 1988. Diurnal variation of bare soil reflectance. ICW note 1854, Wageningen, The Netherlands. p. 19.

BASTIAANSSEN, W.G.M., 1988. New empirical aspects of the Bowen-ratio energy balance method. ICW note 1914, Wageningen, The Netherlands. p. 44.

BASTIAANSSEN, W.G.M. and J.M. HALBERTSMA, 1989. Water flow through unsaturated saline soil. ICW note, Wageningen, The Netherlands. (in preparation).

BASTIAANSSEN, W.G.M. en A. DE GROOT, 1989. Hydrologische bodemklassifikatie volgens een clusteranalyse techniek. ICW note, Wageningen (in preparation).

BAVEL, C.H.M. VAN, and D.I. HILLEL, 1976. Calculating potential and actual evaporation from a bare soil surface by simulation of concurrent flow of water and heat. Agric. Meteorol. 12. p. 361-369.

BELMANS, C., J.G. WESSELING and R.A. FEDDES, 1983. Simulation model of the water balance of a cropped soil: SWATRE. J. Hydrol. 63, 3/4. ICW, Technical bulletin 21, Wageningen, The Netherlands. p. 271-286.

BERGHE, TEN, H.F.M., 1986. Heat and water transfer at the bare soil surface. Thesis, Agricultural University of Wageningen. p. 214.

BLACK, T.A., W.R. GARDNER and G.W. THURTELL, 1969, The prediction of evaporation, drainage and soil water storage for a bare soil. Soil Sci. Soc. Am. Proc. 33, p. 655-660.

BRONSWIJK, J.J.B., 1988. Modeling of water balance, cracking and subsidence of clay soils. J. of Hydrology, 97, p. 199-212.

BRUIN, H.A.R., 1984. Meteorology for hydrologists, Wageningen, The Netherlands, p. 92.

BRUIN, H.A.R., 1987. From Penman to Makkink. TNO-CHO No. 39 p. 5-32.

CARSLAW, H.S. and J.C. JAEGER, 1959. Conduction of heat in solids. p. 510.

FEDDES, R.A., 1971, Water, heat and crop growth. Thesis, Agricultural University, Wageningen, The Netherlands. p. 184.

FEDDES, R.A., P.J. KOWALIK and H. ZARADNY, 1978. Simulation of field water use and crop yield. Simulation monographs, PUDOC, Wageningen, The Netherlands. p. 189.

FEDDES, R.A, P. KABAT, P.J.T. VAN BAKEL, J.J.B. BRONSWIJK and J.HALBERTSMA, 1988. Modelling soil water dynamics in the unsaturated zone, state of art. J. of Hydr., 100 (special issue) p. 69-111.

FORSYTHE, W.E., 1969. Smithsonian physcical tables. Ninth revised edition, Smithsonian Institute, Washington DC. p. 827.

FRITSCHEN, L.J., GAY, L.W., 1979. Environmental instrumentation. p. 213.

GAUDU, J.C., 1988. Mise en oeuvre de la methode psychrometrique de mesure du potentiel de l'eau dans le sol, INRA report, Avignon. p. 32.

GELGAM AD HOC GROEP VERDAMPING, 1984, Herziening van de berekening van de gewasverdamping in het hydrologisch model GELGAM, Rijkswaterstaat, dienst informatieverwerking, Arnhem, The Netherlands. p. 93.

GENUCHTEN, M. TH. VAN, 1980. A closed-form equation for predicting the hydraulic conductivity of unsaturatred soils. Soil Sci. Am. Journal no. 44. p. 892-898.

HAVERKAMP, R., ET AL., 1977. A comparison of numerical simulation models for one-dimensional infiltration. Soil Sci. Soc. Am. Proc., 41. p. 285-294.

HEYS, A., 1987. Analytische en numerieke berekeningen van temperatuursvelden in inhomogene media. Technical College, Eindhoven, The Netherlands. p. 110.

ILRI, Drainage principles and applications, introductory subjects, Publication 16, Vol 1. p. 241.

JACKSON, R.D. ET AL., 1964. Water vapour diffusion in relative dry soil. Soil Sci. Soc. Amer. Proc., 28(2), 28(4), p. 172-176, p. 464-470.

KABAT, P., 1986. Moisture, heat and salts dynamics in fileds with trickler and localized irrigation. Thesis, TU-press, p. 115.

KABAT, P., 1988. Agrohydrological simulation models in drainage. Twenty-seventh international course on land drainage. p. 35.

KABAT P., F.J.E. BOLT and J. BRUGGEMAN, 1988. SWASALT. A simulation model for water and conservative solute transport in the unsaturated zone. Simulation software, ICW, Wageningen.

KABAT, P. and M.J.D. HACK-TEN BROEKE, 1988. Input data for agrohydrological simulation models: some parameter estimation techniques. Proc. of the EC-workshop on EC soil maps and climate data, Wageningen. p. 18.

KABAT, P., J.G. WESSELING, B.J. VAN DEN BROEK and R.A. FEDDES, 1989. SWATRE/SWACROP. A new version of a model to simulate soil water dynamics, evapotranspiration and related crop production. User's manual with some case studies. p. 150 (in preparation) .

LIST, R.J., 1984. Smithsonian Meteorological Tables, fifth reprint. Smithsonian Institute, Washington DC. p. 527.

MARSILY, G., de, 1986. Quantitative hydrogeology, Academic press, p. 440.

MENENTI, M., R. LUPINI and E. ALIVERTI, 1979. Modelli numerici per la previsione del transitorio termico in tubi interrati. Sogesto report, Urbino, Italy. p. 37.

MENENTI, M., 1984. Physical aspects and determinations of evaporation in deserts applying remote sensing techniques. Report no. 10 (special issue), p. 202.

MENENTI, M., W.G.M. BASTIAANSSEN and M.H. ABD EL KARIM, 1987. Determination of groundwater losses by evaporation in the Western desert of Egypt. Proc. ISPRS-Regional congress. Applications of remote sensing in hydrology, Amman 22-26 October, Jordan. p. 13 .

MENENTI, M., W.G.M. BASTIAANSSEN, D. van EICK and M.H. ABD EL KARIM, 1988. Linear relationships between surface reflectance and temperature and their application to map actual evaporation of groundwater. Advances in Space Research (in print). p. 12.

MENENTI, M., W.G.M. BASTIAANSSEN and D. van EICK, 1988. Determination of hemispherical reflectance with Thematic Mapper measurements. Final Workshop NASA TM Science Program; to appear in Rem. Sens. of Env., special issue, p. 27.

MONTEITH, J.L., 1973. Principles of environmental physics, London, p. 241.

NEUMAN, S.P., R.A. FEDDES and E. BRESLER, 1975. Finite element analysis of two-dimensional soil water flow considering water uptake by roots. 1. Theory. Soil Sci. Soc. Am. Proc., 39. p. 224-230.

PHILIP, J.R., 1957. Evaporation, moisture and heat fields in the soil. J. Meteorol. 14: p. 354-366.

ROBINSON, R.A. and STOKES, R.H., 1955. Electric solutions, Butterworths, London. p. 38.

RICHARDS, L.A., 1954, Diagnosis and improvements of saline and alkali soils, United States Salinity Laboratory Staff, Agricultural handbook No.60., United States Department of Agriculture. p. 160.

RITCHIE, J.T. and J.E. ADAMS, 1974. Field measurements of evaporation from soil shrinkage cracks. Soil Sci. Soc. Am. Proc., 38(1). p. 131-134.

VRIES, D.A. de, 1963. Thermal properties of soils, Agricultural University, Wageningen, The Netherlands. p. 211-235.

WEAST, R.C., 1971. Handbook of Chemistry and Physics, 51st edition.

WESSELING, J.G., P. KABAT, B.J. van den BROEK and R.A. FEDDES, 1988. SWACROP, version 1.0. A model to simulate one-dimensional transient soil water flow, evapotranspiration and crop production. Simulation software, ICW, Wageningen.

WÖSTEN, H., LOON, L. van, 1979. A model to simulate evaporation of bare soils in arid regions. Agricultural University, Wageningen. p. 94.

APPENDIX 1

DERIVATION OF MENENTI'S COMBINATION EQUATION

The transport equations for the vertical flux of heat in air and soil can succesively be written as:

$$H = - \frac{\rho_a C_p}{R_{ah}} (T_0 - T_a) \qquad (W.m^{-2}) \qquad [70]$$

$$G_0 = - \frac{(T_0 - T_e)}{R_{sh}} \qquad (W.m^{-2}) \qquad [71]$$

The combined latent heat flux through soil and air, assuming that the latent heat flux between the evaporation front and the soil surface coincides with the latent heat flux through the air layer above the surface, is of the form:

$$LE = - \frac{\rho_a C_p}{\gamma(R_{av}+R_{sv})} (e_{sat}(T_e)-e(z)) \qquad (W.m^{-2}) \qquad [72]$$

The saturated vapour pressure at the evaporation front ($e_{sat}(T_e)$) can be related with the usually applied saturated vapour pressure at screen height ($e_{sat}(T_a)$) including the slope of the saturated vapour pressure curves i.e. $S_a = de_{sat}/dT_a$ and $S_s = de_{sat}/dT_s$:

$$e_{sat}(T_e) = e_{sat}(T_a) + S_a(T_0-T_a) + S_s(T_e-T_0) \qquad (mbar) \qquad [73]$$

Substituting the energy balance equation without latent heat exchange ($Rn+H+G_0 = 0$) and the soil heat flux leaving the surface composed of $(G_0-W_e)+G_e+LE = 0$ one gets:

$$e_{sat}(T_e) = e_{sat}(T_a) + \frac{S_a R_{ah}}{\rho_a C_p} (Rn+LE+G_e+W_e) + S_s R_{sh}(LE+G_e+W_e) \qquad (mbar) \qquad [74]$$

Combination of equation [72] and [74] shows:

$$- \gamma(R_{av}\ R_{sv})LE = \rho_a\ C_p[e_{sat}(T_a - e(z)] + S_a\ R_{ah}(R_n + LE + G_e + W_e) +$$

$$S_s\ \rho_a\ C_p\ R_{sh}(LE + G_e + W_e) \qquad [75]$$

The expression of all variables in terms of latent heat flux, yields the required expression for LE_{act}.

APPENDIX 2

CALCULATION OF POTENTIAL EVAPORATION

When the evaporation front is located at surface level i.e. when z_e = 0.0 cm, the latent heat flux coincides with the definition of the potential evaporation. The potential evaporation concept on itself is quite questionable, because varying soil heat flow, sensible heat advection and the presence of salts are hardly measurable. Nevertheless, the approach is applicable as a maximum possible flux through the surface. Penman (1948) proposed the following combination of aerodynamic transfer fluxes with the surface energy balance equation of an open water surface. V. Bavel (1966) suggested the same formula for land types. Fluxes towards the surface are counted postive:

$$LE = - \frac{\rho_a C_p [e_{sat}(z) - e_{act}(z)]/R_a + S_a(R_n + G_0)}{\gamma + S_a} \qquad (W.m^{-2}) \qquad [76]$$

where LE = Latent heat flux ($W.m^{-2}$)
ρ_a = Air density ($kg.m^{-3}$)
C_p = Air specific heat at constant pressure ($J.kg^{-1}.K^{-1}$)
e_{sat} = Saturated air vapour pressure (mbar)
e_{act} = Actual air vapour pressure (mbar)
S_a = Slope of the saturated air vapour pressure curve ($mbar.K^{-1}$)
R_a = Aerodynamic resistance ($s.m^{-1}$)
R_n = Net radiation ($W.m^{-2}$)
G_0 = Soil heat flux at the surface ($W.m^{-2}$)
γ = Thermodynamic psychrometric constant ($mbar.K^{-1}$)

The net radiaton budget requires for additional elucidation. The net radiation is proposed in a simple form after introduction of an apparent term for the longwave sky radiation (ϵ'):

$$R_n = (1 - \alpha_o) R_{sw} + \epsilon' \sigma T_a^4 - \epsilon \sigma T_0^4 \qquad (W.m^{-2}) \qquad [77]$$

where Rn ($W.m^{-2}$) is the net radiation, α_o(-) the surface reflectance, R_{sw} ($W.m^{-2}$) the incident irradiance, ϵ'(-) the apparent emissivity of the atmosphere, σ($8.67\ 10^{-8}$ $W.m^{-2}.k^{-4}$) the Stefan Boltzmann constant, T_a (K) the air temperature at screen height, ϵ(0.97 (-)) the emissivity of the

soil surface and T_0 (K) the surface temperature. The surface reflectance shows a diurnal variation (eq. [78]), and is an important variable in the estimation of net radiation budget and evaporation rate. So, the surface reflectance is an useful characteristic for remote sensing investigation to study energy processes at the surface (Menenti et al., 1988b). The EVADES-model is able to simulate such physical relationships.

A new empirical equation (Bastiaanssen, 1988a and Menenti et al., 1988b) which relates surface reflectance data (α_0) to solar zenith angle (ϕ_{su}), atmospheric transmittance (τ) and ground conditions such as soil type (m), moisture content (m $f(\phi_{su})$) and roughness (g), is implemented in the current version of the EVADES-model.

$$\alpha_0 = \alpha_0' \; m \; f(\phi_{su}) \; [g(\tau)]^{\sin \phi_{su}} \qquad (-) \qquad [78]$$

where m $f(\phi_{su})$ and $g(\tau)$ (-) are empirical constants for the effect of dew and atmospherical scattering properties respectively and α_o' (-) the surface reflectance at ϕ_{su} = 0.0. Furthermore, the apparent emisivity of the atmosphere was empirically fitted with the actual vapour pressure (Brunt, 1932) after measurements in the Western Desert of Egypt according:

$$\epsilon' = a + b \sqrt{e_{act}} \qquad (-) \qquad [79]$$

where a and b are the regression coefficients being a = 0.72, b = 0.046 and a = 0.61, b = 0.068 for daytime and night time respectively (BASTIAANSSEN, 1988b).

In order to predict the saturated vapour pressure at surface level, the temperature dependent slope of the saturated vapour pressure curve was introduced (Penman, 1948). He considered that the air above an (salt free) open water surface was saturated and that the required saturated vapour pressure could be derived from air temperature recordings:

$$e_{sat}(T_0) = e_{sat}(T_a) + S_a \; (T_0 - T_a) \qquad \text{with} \qquad (\text{mbar}) \qquad [80]$$

$$S_a = \frac{4093.4 \; e_{sat}}{(237.3 + T)^2} \qquad (\text{mbar.K}^{-1}) \qquad [81]$$

where S_a (mbar.K^{-1}) is the slope of the saturated air vapour pressure

curve, e_{sat} (mbar) the saturated vapour pressure and T (°C) the temperature. The thermodynamic psychrometric constant (γ) (mbar.k^{-1}) varies with temperature because the latent heat of vaporization (L) (J.kg^{-1}) varies with temperature (T) (°C):

$$L = (2501 - T\ 71/30) \qquad (10^3\ J.kg^{-1}) \qquad [82]$$

$$\gamma = \left(\frac{1004\ 461}{287\ L}\right)P \qquad (mbar.K^{-1}) \qquad [83]$$

Particular theories of the atmospheric resistance are seperated and presented in appendix 3.

APPENDIX 3

ATMOSPHERIC RESISTANCES TO HEAT AND VAPOUR TRANSFER

The lower part of the atmosphere where the physical processes of the atmosphere are affected by the surface, is called the atmospheric boundary layer. The vertical vapour and temperature profiles in the turbulent atmospheric boundary layer can be among others described by means of the aerodynamic resistance (R_a). The turbulent atmosphere has different stability conditions. The air stabilitity can be evaluated with the gradient of air temperature. If this gradient dT_a/d_z equals 6.5 Kelvin per kilometer, there is no heat exchange with the surrounding air (adiabatic process). This is the theoretical defenition of neutral condition. More practically, one may assume that the neutral stratification is reached when the surface and air temperature are of the same order of magnitude ($T(z) \approx T_0$). This is more likely with potential evaporation then in cases of actual evaporation. In unstable conditions, temperature decreases with height, while in stable conditions the situation is otherwise. When the actual evaporation is reduced by the vapour transfer through the topsoil, the atmosphere is certainly assumed to be unstable which induces large differences in temperature ($T_0 \neq T(z)$).

The vertical flux of momentum can be written in the form:

$$\tau = - \rho \frac{\partial u(z)}{R_{am}} \qquad (N) \qquad [84]$$

where τ(N) is the shear stress, u ($m.s^{-1}$) the windspeed at height z and R_{am} ($s.m^{-1}$) the aerodynamic resistance to momentum. The shear stress on turn is determined from the friction velocity (u*) ($m.s^{-1}$) and density ($kg.m^{-3}$) according:

$$\tau = \rho u^{*2} \qquad (N) \qquad [85]$$

Hence, the aerodynamic resistance to momentum can be simple written as $R_{am} = [u(z2)-u(z1)]/u^{*2}$. The friction velocity can be calculated on basis of eq. [86].
The term ϕ_m becomes one when the atmosphere is neutral.

$$u^* = k(\bar{z}-d)\ \phi_m^{-1}\ \frac{\partial u}{\partial z} \qquad (m.s^{-1}) \qquad [86]$$

where u ($m.s^{-1}$) is the windspeed, z (m) the height, u* ($m.s^{-1}$) the friction velocity, k (-) the von karman constant (0.41) and d (m) the zero plane displacement. The latter parameter can be empirically related with the vegetation lenght of a uniform crop e.g. 0.63 times the vegetation height (Monteith, 1973). The logarithmic windprofile follows after the integration of eq. [86] with respect to depth:

$$u(z2)-u(z1) = \frac{u^*\phi_m}{k}\ \ln(\frac{z2-d}{z1-d}) \qquad (m.s^{-1}) \qquad [87]$$

Mathematically seen, z1 is the elevation where the windspeed u(z1) becomes zero. Hence, z1 is the roughness length ($m.s^{-1}$) just above the surface. The roughness length varies for different surface types. In cases of roughness length above a bare soil surface, a value of z1 = 0.005 m can be considered (de Bruin, 1984). Combination of eq. [84], [85] and eq. [87] yields the required expression for aerodynamic resistance under neutral stratification:

$$R_{am} = R_{ah} = R_{av} = \frac{1}{k\ u^*}\ \ln(\frac{z2-d}{z1-d}) \qquad (s.m^{-1}) \qquad [88]$$

or in terms of wind velocity:

$$R_{am} = R_{ah} = R_{av} = \frac{1}{k^2\ (u(z2)-u(z1))}\ [\ln(\frac{z2-d}{z1-d})]^2 \qquad (s.m^{-1}) \qquad [89]$$

The temperature profile is surely non-neutral, when the evaporation front is located inside the soil ($LE_{act} << LE_{pot}$). A measure for stability is given by the Monin-Obukov stability parameter or the Richardson number (Ri). The condition of air thermal stratification can be expressed by evaluation of the easy measurable Richardson number (Ri):

$$Ri = \frac{g(\partial Ta/\partial z)}{\overline{T_a}(\partial U/\partial z)^2} \qquad (-) \qquad [90]$$

The unstable condition applies when the Richardson number is negative. The ratio R_{ah}/R_{av} is different from unity under a non-neutral conditions. For this reason, different flux profile relationships (ϕ-functions) for

heat and vapour transport through a non-neutral atmosphere have to be distinguished.

The ϕ-functions are derived for layers where the energy fluxes are constant with height, so that the air layer at the soil surface (i.e. by taking the surface temperature) may not be considered in the calculation of the Richardson number. A summary is presented in table 9:

Table 9. Flux-profile relationships; Monin-Obukov's ϕ-functions applied in the EVADES-model

	Stable condition	Unstable condition	Neutral condition
definition	$dT_a/dz>6.5$ K.km^{-1}	$dT_a/dz<6.5$ K.km^{-1}	$dT_a/dz=6.5$ K.km^{-1}
T_a-profile	$T_a>T_0$	$T_a<T_0$	$T_a=T_0$
evaporation	e_{act}	e_{act}	$\tilde{e}_{pot}$
Richardson	Ri>0	Ri<0	Ri=0
ϕheat	$\phi_h=0.885(1+34Ri)^{0.40}$	$\phi_h=0.885(1-22Ri)^{-0.40}$	$\phi_h=1.0$
ϕvapour	$\phi_v=0.950(1+16Ri)^{0.33}$	$\phi_v=(1-16Ri)^{-0.25}$	$\phi_v=1.0$

The friction velocities (u*) for transport of heat and vapour in turbulent air can now be calculated with eq. [87], applying the above specified ϕ-functions. Monteith (1981) suggested to write finally the resistance transport factors as:

$$R_x = b_x^{-1} \int_{z1}^{z2} (u^* z-d)^{-1} \phi_x \, dz \qquad (s.m^{-1}) \qquad [91]$$

After an integration with respect to height, the resistance for heat and vapour transfer can respectively be written analogous with eq. [88] as:

$$R_{ah} = \frac{1}{k} \frac{\phi_v}{u^*v} \ln\left(\frac{z2-d}{z1-d}\right) \qquad (s.m^{-1}) \qquad [92]$$

$$R_{av} = \frac{1}{k} \frac{\phi_h}{u^*h} \ln\left(\frac{z2-d}{z1-d}\right) \qquad (s.m^{-1}) \qquad [93]$$

APPENDIX 4

DIURNAL VARIATION OF METEOROLOGICAL VARIABLES

Calculating the evaporation rate in time steps less than one day, the course of meteorological variables during the day has to be known. Most meteorological variables have a clear diurnal cyclus. Some of them have even a predictable trend. This especially holds true with cloudless skies, like in arid regions. Then the net radiation, which is the source of all energy processes, has a clear sinusoidal shape with time (see Fig. 16). As a consequence, the surface temperature, air temperature and relative humidity follow this trend during daytime.

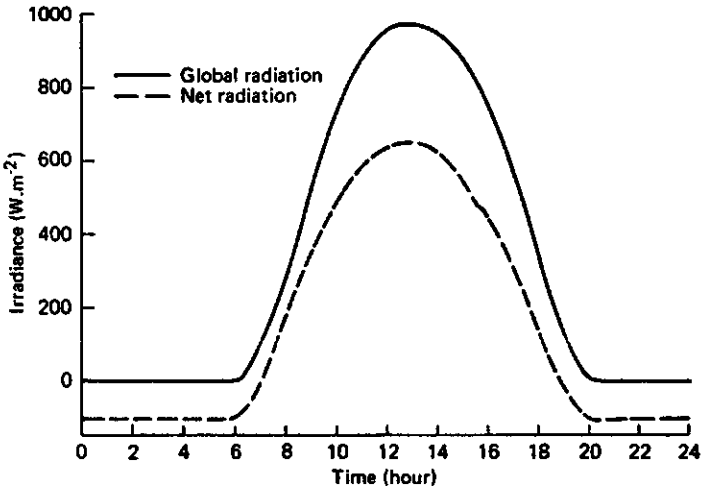

Fig. 16. Diurnal variation of net- and global radiation as measured at Bir Qifar in the Western Desert of Egypt on 24 June 1988

Cooling down processes by the difference between emitted thermal radiation from the atmosphere and the surface at night, result in negative net radiation values and dew point temperatures at the soil surface. This makes the amplitudes of the meteorological variables during the night lower then during the day. Hence, sinusoidal functions considering the complete period of one day has to be substituted by two half-sinusoidal functions with different amplitudes.

Global radiation and surface temperature generally response directly to the zenith angle of the sun so that the maximum values are reached at the lowest zenith angle. Values at sunsrise and sunset has to be prescribed. This is applied in the following equations:

$$R_{sw}(t) = R_{sw}max \sin(\pi t/P1) \quad t_{sunr.} \leq t \leq t_{sunset} \quad (W.m^{-2}) \quad [94]$$

$$R_{sw}(t) = 0 \quad t_{sunset} \leq t \leq t_{sunr.} \quad (W.m^{-2}) \quad [95]$$

$$T_0(t) = T_0sunr.+(T_0max-T_0sunr.) \sin(\pi t/P1) \quad t_{sunr.} \leq t \leq t_{sunset} \quad (K) \quad [96]$$

$$T_0(t) = T_0sunr.-(T_0sunset-T_0min) \sin(\pi t/P2) \quad t_{sunset} \leq t \leq t_{sunr.} \quad (K) \quad [97]$$

Due to time lag effects, the half-sinusoidal functions of air temperature and relative humidity often not comprises the periods between sunrise and sunset. Therefore the approach to estimate soil temperature as outlined in section 3.2.3 is followed. This concerns the variation of the air temperature and the relative humidity as follows:

$$T_a(t) = \overline{T_a} + A(T_a)1 \sin(\pi t/P1) \quad T_a(t) \geq T_a \quad (K) \quad [98]$$

$$T_a(t) = \overline{T_a} - A(T_a)2 \sin(\pi t/P2) \quad T_a(t) \leq T_a \quad (K) \quad [99]$$

$$U(t) = \overline{U} + A(U)1 \sin(\pi t/P1) \quad U(t) \geq U \quad (-) \quad [100]$$

$$U(t) = \overline{U} - A(U)2 \sin(\pi t/P2) \quad U(t) \leq U \quad (-) \quad [101]$$

where $\overline{T_a}$, $\overline{U}$ are the daily average values and $A(T_a)x$, $A(U)x$ the amplitudes of the period considered. The diurnal variation of windspeed is unpredictable, since it is affected by large scale weather systems. However, a general ratio between the day- and nighttime is often considered for the calculation of the average daily windspeed. The ratio U_{day}/U_{night} can be given is an input parameter. Observations in hyper-arid regions like the Western Desert of Egypt showed values of U_{day}/U_{night}=1.3. Latter ratio shows no approved relation with the height above the surface.

APPENDIX 5

TEMPERATURE RELATED PROPERTIES OF LIQUID WATER

A. density

T(°C)	ρ_w(gr.cm^{-3})	T(°C)	ρ_w(gr.cm^{-3})	T(°C)	ρ_w(gr.cm^{-3})	T(°C)	ρ_w(gr.cm^{-3})
-20	0.99349	16	0.998972	48	0.988957	80	0.971819
-18	0.99474	17	0.998804	49	0.988515	81	0.971193
-16	0.99581	18	0.998625	50	0.988066	82	0.970562
-14	0.99672	19	0.998435	51	0.987610	83	0.969926
-12	0.99749	20	0.998234	52	0.987148	84	0.969286
-10	0.998137	21	0.998022	53	0.986680	85	0.968640
- 9	0.998417	22	0.997801	54	0.986205	86	0.967990
- 8	0.998671	23	0.997569	55	0.985723	87	0.967335
- 7	0.998899	24	0.997327	56	0.985236	88	0.966674
- 6	0.999102	25	0.997075	57	0.984743	89	0.966009
- 5	0.999283	26	0.996814	58	0.984243	90	0.965340
- 4	0.999441	27	0.996544	59	0.983737	91	0.964665
- 3	0.999578	28	0.996264	60	0.983226	92	0.963986
- 2	0.999694	29	0.995976	61	0.982708	93	0.963302
- 1	9.999790	30	0.995678	62	0.982185	94	0.962613
0	0.999868	31	0.995372	63	0.981655	95	0.961920
1	0.999927	32	0.995057	64	0.981120	96	0.961222
2	0.999968	33	0.994734	65	0.980580	97	0.960519
3	0.999992	34	0.994403	66	0.980034	98	0.959812
4	1.000000	35	0.994063	67	0.979482	99	0.959100
5	0.999992	36	0.993716	68	0.978924	100	0.958384
6	0.999968	37	0.993360	69	0.978361	101	0.957662
7	0.999930	38	0.992997	70	0.977793	102	0.956937
8	0.999877	39	0.992626	71	0.977219	103	0.956207
9	0.999809	40	0.992247	72	0.976640	104	0.955472
10	0.999728	41	0.991861	73	0.976056	105	0.954733
11	0.999634	42	0.991467	74	0.975466	106	0.953989
12	0.999526	43	0.991067	75	0.974871	107	0.953240
13	0.999406	44	0.990659	76	0.974271	108	0.952488
14	0.999273	45	0.990244	77	0.973665	109	0.951730
15	0.999129	46	0.989822	78	0.973055	110	0.950968
		47	0.989393	79	0.972439		

After Handbook of Chemistry and Physics. Table F-5

B. Surface tension of water against air

T(°C)	σ_{wa} dynes/cm	T(°C)	σ_{wa} dynes/cm	T(°C)	σ_{wa} dynes/cm	T(°C)	σ_{wa} dynes/cm	T(°C)	σ_{wa} dynes/cm	T(°C)	σ_{wa} dynes
0	75.69	11	74.07	21	72.59	31	71.02	41	69.40	51	67.74
1	75.46	12	73.93	22	72.44	32	70.86	42	69.23	52	67.56
2	75.32	13	73.78	23	72.28	33	70.69	43	69.07	53	67.39
3	75.18	14	73.64	24	72.13	34	70.53	44	68.90	54	67.22
4	75.04	15	73.49	25	71.97	35	70.37	45	68.74	55	67.05
5	74.90	16	73.34	26	71.81	36	70.21	46	68.57	56	66.87
6	74.76	17	73.20	27	71.65	37	70.05	47	68.41	57	66.70
7	74.63	18	73.05	28	71.50	38	69.88	48	68.24	58	66.53
8	74.49	19	72.90	29	71.34	39	69.72	49	68.08	59	66.35
9	74.36	20	72.75	30	71.18	40	69.56	50	67.91	60	66.18
10	74.22										

After Handbook of Chemistry and Physics, Table F-30

C. Viscosity

T(°C)	η_ω(cp)	T(°C)	η_ω(cp)	T(°C)	η_ω(cp)	T(°C)	η_ω(cp)	η_ω(cp)
0	1.787	26	0.8705	52	0.5290	78	0.3638	ω = fout
1	1.728	27	0.8513	53	0.5204	79	0.3592	W = goed
2	1.671	28	0.8327	54	0.5121	80	0.3547	
3	1.618	29	0.8148	55	0.5040	81	0.3503	
4	1.567	30	0.7975	56	0.4961	82	0.3460	
5	1.519	31	0.7808	57	0.4884	83	0.3418	
6	1.472	32	0.7647	58	0.4809	84	0.3377	
7	1.428	33	0.7491	59	0.4736	85	0.3337	
8	1.386	34	0.7340	60	0.4665	86	0.3297	
9	1.346	35	0.7194	61	0.4596	87	0.3259	
10	1.307	36	0.7052	62	0.4528	88	0.3221	
11	1.271	37	0.6915	63	0.4462	89	0.3184	
12	1.235	38	0.6783	64	0.4398	90	0.3147	
13	1.202	39	0.6654	65	0.4335	91	0.3111	
14	1.169	40	0.6529	66	0.4273	92	0.3076	
15	1.139	41	0.6408	67	0.4213	93	0.3042	
16	1.109	42	0.6291	68	0.4155	94	0.3008	
17	1.081	43	0.6178	69	0.4098	95	0.2975	
18	1.053	44	0.6067	70	0.4042	96	0.2942	
19	1.027	45	0.5960	71	0.3987	97	0.2911	
20	1.002	46	0.5856	72	0.3934	98	0.2879	
21	0.9779	47	0.5755	73	0.3882	99	0.2848	
22	0.9548	48	0.5656	74	0.3831	100	0.2818	
23	0.9325	49	0.5561	75	0.3781			
24	0.9111	50	0.5468	76	0.3732			
25	0.8904	51	0.5378	77	0.3684			

After Handbook of Chemistry and Physics, Table F-36

APPENDIX 6

SALT EFFECTS ON SOIL HYDRAULIC PARAMETERS

The partial derivatives of the matric pressure head and the unsaturated hydraulic conductivity with respect to solute concentration are as follows:

$$\frac{\partial h_m}{\partial C} = \frac{\rho_w \, h_m}{\sigma_{wa}} \frac{\partial}{\partial C} \left(\frac{\sigma_{wa}}{\rho_w}\right) \qquad (m^4.mol^{-1}) \qquad [102]$$

$$\frac{\partial K(h_m)}{\partial C} = \frac{\rho_w \, g \, k}{\eta_w} \frac{\partial b(h_m)}{\partial h_m} \frac{\partial h_m}{\partial C} + g \, K \, b(h_m) \frac{\partial}{\partial C} \left(\frac{\rho_w}{\eta_w}\right) \qquad (m^4.s^{-1}.mol^{-1}) \qquad [103]$$

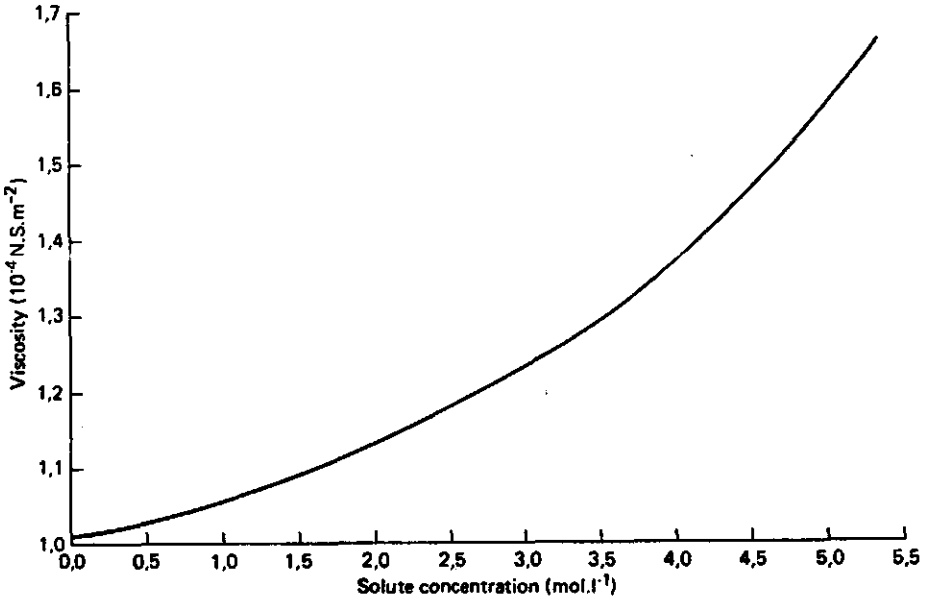

Fig. 17. Relationship between the solute concentration and the viscocity of the water

C mol.l^{-1}	ρ_w gr.cm^{-3}	η_w 10^{-4} N.S.M^{-2}	C mol.l^{-1}	ρ_w gr.cm^{-3}	η_w 10^{-4} N.S.M^{-2}	C mol.l^{-1}	ρ_w gr.cm^{-3}	η_w 10^{-4} N.S.M^{-2}
0.017	0.9989	1.005	0.541	1.0203	1.033	1.407	1.0544	1.082
0.034	0.9997	1.006	0.559	1.0211	1.033	1.445	1.0559	1.084
0.051	1.0004	1.007	0.577	1.0218	1.034	1.484	1.0574	1.087
0.069	1.0011	1.008	0.595	1.0225	1.035	1.522	1.0588	1.090
0.086	1.0018	1.009	0.613	1.0232	1.036	1.560	1.0603	1.093
0.103	1.0025	1.011	0.631	1.0239	1.037	1.599	1.0618	1.096
0.120	1.0032	1.012	0.649	1.0246	1.037	1.637	1.0633	1.099
0.137	1.0039	1.013	0.667	1.0254	1.038	1.676	1.0647	1.102
0.155	1.0046	1.014	0.685	1.0261	1.039	1.715	1.0662	1.105
0.172	1.0053	1.015	0.703	1.0268	1.040	1.754	1.0677	1.108
0.189	1.0060	1.016	0.721	1.0275	1.041	1.793	1.0692	1.111
0.207	1.0068	1.017	0.739	1.0282	1.042	1.832	1.0707	1.115
0.224	1.0075	1.017	0.757	1.0290	1.043	1.930	1.0744	1.123
0.241	1.0082	1.018	0.775	1.0297	1.044	2.029	1.0781	1.132
0.259	1.0089	1.019	0.794	1.0304	1.045	2.129	1.0819	1.142
0.276	1.0096	1.020	0.812	1.0311	1.046	2.229	1.0857	1.152
0.294	1.0103	1.021	0.830	1.0318	1.046	2.330	1.0894	1.162
0.311	1.0110	1.022	0.848	1.0326	1.047	2.432	1.0932	1.173
0.329	1.0117	1.022	0.866	1.0333	1.048	2.534	1.0970	1.184
0.346	1.0125	1.023	0.885	1.0340	1.049	2.637	1.1008	1.196
0.364	1.0132	1.024	0.921	1.0355	1.052	2.741	1.1047	1.207
0.382	1.0139	1.025	0.958	1.0369	1.054	2.845	1.1085	1.219
0.399	1.0146	1.026	0.995	1.0384	1.056	3.056	1.1162	1.243
0.418	1.0153	1.027	1.032	1.0398	1.058	3.270	1.1240	1.267
0.435	1.0160	1.028	1.069	1.0413	1.060	3.486	1.1319	1.293
0.452	1.0168	1.028	1.106	1.0427	1.062	3.706	1.1398	1.322
0.470	1.0175	1.029	1.144	1.0442	1.065	3.928	1.1478	1.357
0.488	1.0182	1.030	1.181	1.0456	1.067	4.153	1.1558	1.396
0.505	1.0189	1.031	1.218	1.0471	1.069	4.382	1.1640	1.441
0.523	1.0196	1.032	1.256	1.0486	1.072	4.613	1.1721	1.489
			1.294	1.0500	1.074	4.848	1.1804	1.542
			1.331	1.0515	1.077	5.085	1.1887	1.600
			1.369	1.0530	1.079	5.326	1.1972	1.662

after Handbook of Chemistry and Physics, Table D-261

APPENDIX 7

FINITE DIFFERENCE SCHEME

$$1.\quad \frac{\rho v_j^{i+1} - \rho v_j}{\Delta t^i} = \frac{1}{\Delta z_j}\left\{Dv^i_{j-\frac{1}{2}}\left(\frac{\Delta \rho v}{\Delta z \mu}\right)^{i+1}_{j-\frac{1}{2}}\right\} - \left\{Dv^i_{j+\frac{1}{2}}\left(\frac{\Delta \rho v}{\Delta z 1}\right)^{i+1}_{j+\frac{1}{2}}\right\}$$

$$2.\quad \frac{\Delta \rho v}{\Delta t^i} = \frac{\rho v_j^{i+1} - \rho_j^i}{\Delta t^i}$$

$$3.\quad \left(\frac{\Delta \rho v}{\Delta z}\right)^{i+1}_{j-\frac{1}{2}} = \frac{(\rho v_{j-1}^{i+1} - \rho v_j^{i+1})}{\Delta z \mu}$$

$$4.\quad \left(\frac{\Delta \rho v}{\Delta z 1}\right)^{i+1}_{j+\frac{1}{2}} = \frac{\rho v_j^{i+1} - \rho v_j^{i+1}}{\Delta z 1}$$

$$5.\quad \frac{\rho v_j^{i+1} - \rho v_j^i}{\Delta t^i} = \frac{1}{\Delta z j}\left\{Dv^i_{j-\frac{1}{2}}\left(\frac{\rho v_{j-1}^{i+1} - \rho v_j^{i+1}}{\Delta z \mu}\right)\right\} - \frac{1}{\Delta z 1}\left\{Dv^i_{j+\frac{1}{2}}\left(\frac{\rho v_j^{i+1} - \rho v_{j+1}^{i+1}}{\Delta z 1}\right)\right\}$$

$$6.\quad \rho v_j^{i+1} - \rho v_j^i = \frac{\Delta t^i}{\Delta z j\ \Delta z \mu}\left\{Dv^i_{j-\frac{1}{2}}\left(\rho v_{j-1}^{i+1} - \rho v_j^{i+1}\right)\right\} - \frac{\Delta t^i}{\Delta z j\ \Delta z 1}\left\{Dv^i_{j+\frac{1}{2}}\left(\rho v_j^{i+1} - \rho v_{j+1}^{i+1}\right)\right\}$$

$$7.\quad \left(\frac{\Delta t^i}{\Delta z j\ \Delta z u} Dv^i_{j+\frac{1}{2}}\right) \rho v_{j+1}^{i+1} + \left(1 + \frac{\Delta t^i}{\Delta z^i\ \Delta z \mu} Dv^i_{j-\frac{1}{2}} + \frac{\Delta t^i}{\Delta z^i \Delta z 1} Dv^i_{j+\frac{1}{2}}\right) \rho v_j^{i+1} -$$

$$- \left(\frac{\Delta t^i}{\Delta z j\ \Delta z_u} Dv^j_{i-\frac{1}{2}}\right) \rho v_{j-1}^{i+1} = \rho v_j^i$$

Equation 7 is the linear Thomas trio-algorithm looked for:

$$8.\quad - A_j\ \rho v_{j+1}^{i+1} + B_j\ \rho v_j^{i+1} - D_j\ \rho v_{j-1}^{i+1} = E_j$$

with

$$A_j = \frac{\Delta t^i}{\Delta z j\ \Delta z 1} Dv^i_{j+\frac{1}{2}}$$

$$B_j = 1 + \frac{\Delta t^i}{\Delta zj\ \Delta z\mu} Dv^i_{j-\frac{1}{2}} + \frac{\Delta t^i}{\Delta zj\ \Delta zl} Dv^i_{j+\frac{1}{2}}$$

$$D_j = \frac{\Delta t^i}{\Delta zj\ \Delta z\mu} Dv^i_{j-\frac{1}{2}}$$

$$E_j = \rho v^i_j$$

APPENDIX 8

EXAMPLE INPUT- AND OUTPUT FILES

SIMULATION MODEL OF BARE SOIL EVAPORATION IN DESERTS (E V A D E S)
version march 1988

outputfile :EVADES.EX

day	hour	gwlo	ze	epot	eact	flxs(1)	rsv	rsh	press.head(ze)	hm(ze)
-	-	cm	cm	cm.day-1	cm.day-1	cm.day-1/kg.m-2.s-1	s.m-1	s.m-1	cm	cm

HOMOGENEOUS SALINE SAND PROFILE, SUMMERPERIOD, QATTARA DEPRESSION

56	1	-38.	0.175	0.118E+00	0.431E+00	0.384E+04	0.655E+00	0.624E-03	-0.215E+03	-0.324E+05
56	1	-38.	0.617	0.118E+00	0.461E+00	0.825E+02	0.281E+01	0.221E-02	-0.215E+03	-0.324E+05
56	2	-38.	4.766	0.187E+00	-0.464E+00	0.445E+03	0.236E+02	0.276E-01	-0.147E+07	-0.327E+05
56	3	-38.	6.873	0.207E+00	-0.231E+00	0.332E+03	0.454E+02	0.474E-01	-0.553E+07	-0.331E+05
56	4	-38.	9.489	0.186E+00	-0.566E-01	0.325E+03	0.107E+04	0.955E-01	-0.177E+07	-0.334E+05
56	5	-38.	11.838	0.384E+00	0.103E-01	0.316E+03	0.787E+03	0.113E+00	-0.332E+07	-0.337E+05
56	6	-38.	13.979	0.128E+00	-0.139E-01	0.307E+03	0.469E+03	0.126E+00	-0.465E+07	-0.339E+05
56	7	-38.	16.049	0.363E+00	0.863E-01	0.379E+03	0.445E+03	0.146E+00	-0.284E+06	-0.331E+05
56	8	-38.	17.813	0.518E+00	0.189E+00	0.451E+03	0.444E+03	0.160E+00	-0.464E+07	-0.326E+05
56	9	-38.	19.477	0.726E+00	0.285E+00	0.517E+03	0.588E+03	0.177E+00	-0.330E+07	-0.322E+05
56	10	-38.	20.302	0.101E+01	0.304E+00	0.570E+03	0.433E+03	0.181E+00	-0.142E+06	-0.319E+05
56	11	-38.	20.423	0.132E+01	0.417E+00	0.584E+03	0.419E+03	0.181E+00	-0.153E+06	-0.317E+05
56	12	-38.	20.432	0.147E+01	0.472E+00	0.592E+03	0.408E+03	0.181E+00	-0.155E+06	-0.316E+05
56	13	-38.	20.434	0.143E+01	0.466E+00	0.593E+03	0.401E+03	0.181E+00	-0.156E+06	-0.316E+05
56	14	-38.	20.433	0.115E+01	0.405E+00	0.586E+03	0.398E+03	0.181E+00	-0.155E+06	-0.315E+05
56	15	-38.	20.427	0.841E+00	0.278E+00	0.571E+03	0.397E+03	0.181E+00	-0.153E+06	-0.315E+05
56	16	-38.	20.413	0.693E+00	0.122E+00	0.536E+03	0.405E+03	0.181E+00	-0.149E+06	-0.315E+05
56	17	-38.	20.380	0.581E+00	-0.569E-02	0.476E+03	0.420E+03	0.181E+00	-0.140E+06	-0.316E+05
56	18	-38.	20.320	0.562E+00	-0.823E-01	0.393E+03	0.434E+03	0.180E+00	-0.125E+06	-0.319E+05
56	19	-38.	20.226	0.648E+00	-0.148E+00	0.287E+03	0.444E+03	0.180E+00	-0.106E+06	-0.322E+05
56	20	-38.	20.043	-0.145E+01	-0.910E-01	0.262E+03	0.406E+03	0.180E+00	-0.796E+05	-0.337E+05
56	21	-38.	20.065	-0.102E+01	-0.170E+00	0.281E+03	0.432E+03	0.180E+00	-0.826E+05	-0.336E+05
56	22	-38.	20.102	-0.561E+00	-0.104E+00	0.296E+03	0.458E+03	0.180E+00	-0.880E+05	-0.335E+05
56	23	-38.	20.129	0.121E+00	-0.185E-01	0.307E+03	0.482E+03	0.180E+00	-0.923E+05	-0.335E+05
56	24	-38.	20.148	0.512E-02	-0.866E-01	0.315E+03	0.505E+03	0.180E+00	-0.956E+05	-0.335E+05
57	1	-38.	20.161	0.118E+00	-0.106E+00	0.326E+03	0.528E+03	0.180E+00	-0.979E+05	-0.335E+05
57	2	-38.	20.180	0.187E+00	-0.106E+00	0.327E+03	0.542E+03	0.180E+00	-0.101E+06	-0.335E+05
57	3	-38.	20.180	0.207E+00	-0.933E-01	0.324E+03	0.554E+03	0.180E+00	-0.102E+06	-0.335E+05
57	4	-38.	20.176	0.186E+00	-0.701E-01	0.319E+03	0.568E+03	0.180E+00	-0.101E+06	-0.336E+05
57	5	-38.	20.169	0.384E+00	0.135E-01	0.312E+03	0.583E+03	0.180E+00	-0.100E+06	-0.337E+05
57	6	-38.	20.158	0.128E+00	0.147E-02	0.304E+03	0.597E+03	0.180E+00	-0.982E+05	-0.337E+05
57	7	-38.	20.157	0.374E+00	0.644E-01	0.379E+03	0.553E+03	0.180E+00	-0.962E+05	-0.332E+05
57	8	-38.	20.257	0.552E+00	0.167E+00	0.451E+03	0.508E+03	0.180E+00	-0.114E+06	-0.327E+05
57	9	-38.	20.333	0.792E+00	0.317E+00	0.517E+03	0.466E+03	0.181E+00	-0.130E+06	-0.322E+05
57	10	-38.	20.388	0.112E+01	0.514E+00	0.570E+03	0.433E+03	0.181E+00	-0.143E+06	-0.319E+05
57	11	-38.	20.424	0.145E+01	0.696E+00	0.584E+03	0.419E+03	0.181E+00	-0.153E+06	-0.317E+05
57	12	-38.	20.432	0.161E+01	0.792E+00	0.592E+03	0.409E+03	0.181E+00	-0.155E+06	-0.316E+05
57	13	-38.	20.434	0.157E+01	0.798E+00	0.593E+03	0.402E+03	0.181E+00	-0.156E+06	-0.316E+05
57	14	-38.	20.433	0.128E+01	0.711E+00	0.586E+03	0.398E+03	0.181E+00	-0.155E+06	-0.315E+05
57	15	-38.	20.427	0.940E+00	0.526E+00	0.571E+03	0.397E+03	0.181E+00	-0.153E+06	-0.315E+05
57	16	-38.	20.413	0.766E+00	0.288E+00	0.536E+03	0.406E+03	0.181E+00	-0.149E+06	-0.315E+05
57	17	-38.	20.380	0.623E+00	0.802E-01	0.476E+03	0.420E+03	0.181E+00	-0.140E+06	-0.316E+05
57	18	-38.	20.320	0.580E+00	-0.551E-01	0.393E+03	0.435E+03	0.180E+00	-0.125E+06	-0.319E+05
57	19	-38.	20.226	0.644E+00	-0.165E+00	0.287E+03	0.445E+03	0.180E+00	-0.106E+06	-0.322E+05
57	20	-38.	20.043	-0.145E+01	-0.910E-01	0.262E+03	0.407E+03	0.180E+00	-0.796E+05	-0.337E+05
57	21	-38.	20.065	-0.102E+01	-0.170E+00	0.281E+03	0.433E+03	0.180E+00	-0.826E+05	-0.336E+05
57	22	-38.	20.102	-0.561E+00	-0.104E+00	0.296E+03	0.459E+03	0.180E+00	-0.880E+05	-0.335E+05
57	23	-38.	20.129	0.121E+00	-0.185E-01	0.307E+03	0.483E+03	0.180E+00	-0.923E+05	-0.335E+05
57	24	-38.	20.148	0.512E-02	-0.866E-01	0.315E+03	0.505E+03	0.180E+00	-0.956E+05	-0.335E+05
58	1	-38.	20.161	0.118E+00	-0.106E+00	0.326E+03	0.529E+03	0.180E+00	-0.979E+05	-0.335E+05

SIMULATION MODEL OF BARE SOIL EVAPORATION IN DESERTS (E V A D E S)
version march 1988

outputfile :EVADES.POT

day	hour	sd	rnrad	gOin	rhoair	vpd	rav	rah	u*	ri	psych	rle0	temp(1)	rh
-	-	mbar.k-1	w.m-2		kg.m-3	mbar	s.m-1		m.s-1	-	mbar.k-1	w.m-2	c	-

HOMOGENEOUS SALINE SAND PROFILE, SUMMERPERIOD, QATTARA DEPRESSION

56	1	0,80	-149.3	170.8	1.251	6.965	271.079	271.079	0.02145	-1.309	0.664	-33.84	10.50	0.418
56	2	0.77	-142.6	209.3	1.252	6.340	311.697	311.697	0.02001	-1.567	0.664	-53.72	10.06	0.455
56	3	0.77	-134.9	214.1	1.252	5.917	311.703	311.703	0.02001	-1.567	0.664	-59.25	10.06	0.491
56	4	0.80	-126.2	190.9	1.250	5.659	271.098	271.098	0.02145	-1.309	0.664	-53.19	10.50	0.527
56	5	0.90	-113.6	147.6	1.240	5.973	52.687	52.687	0.04866	-0.129	0.666	-109.83	12.53	0.564
56	6	1.07	-98.7	93.8	1.227	6.640	119.549	119.549	0.04171	0.567	0.668	-36.43	15.50	0.600
56	7	1.38	84.9	8.0	1.206	9.589	139.170	139.170	0.03865	0.692	0.671	-103.17	20.17	0.569
56	8	1.75	217.2	-72.8	1.187	13.417	156.511	156.511	0.03645	0.806	0.673	-146.41	24.56	0.538
56	9	2.13	355.3	-143.9	1.170	17.969	170.991	170.991	0.03487	0.903	0.676	-204.47	28.43	0.508
56	10	2.49	505.2	-201.1	1.157	22.825	182.183	182.183	0.03378	0.980	0.678	-284.95	31.55	0.477
56	11	2.64	627.2	-223.4	1.153	25.886	186.450	186.450	0.03340	1.010	0.679	-369.61	32.77	0.446
56	12	2.77	687.8	-241.2	1.149	28.842	189.794	189.794	0.03310	1.033	0.679	-411.09	33.73	0.415
56	13	2.86	684.3	-254.0	1.147	31.565	192.197	192.197	0.03289	1.050	0.680	-401.12	34.43	0.385
56	14	2.92	610.9	-282.4	1.146	33.932	193.644	193.644	0.03277	1.060	0.680	-322.49	34.86	0.354
56	15	2.92	479.8	-261.8	1.147	35.548	193.645	193.645	0.03277	1.060	0.680	-235.46	34.86	0.323
56	16	2.77	316.4	-151.2	1.152	34.915	189.797	189.797	0.03310	1.033	0.679	-194.31	33.73	0.292
56	17	2.49	151.0	-26.4	1.161	32.226	182.186	182.186	0.03378	0.980	0.678	-163.02	31.55	0.262
56	18	2.13	12.2	105.4	1.175	28.078	170.995	170.995	0.03487	0.903	0.676	-158.28	28.43	0.231
56	19	1.75	-149.3	301.4	1.191	23.258	156.517	156.517	0.03645	0.806	0.673	-183.20	24.56	0.200
56	20	1.07	-177.3	-529.5	1.229	12.676	439.752	439.752	0.01684	1.575	0.668	414.31	15.50	0.236
56	21	1.07	-168.9	-335.7	1.229	12.072	439.752	439.752	0.01684	1.575	0.668	290.93	15.50	0.273
56	22	0.98	-164.6	-162.0	1.236	10.379	231.650	231.650	0.02321	0.690	0.667	160.21	13.95	0.309
56	23	0.90	-160.1	-16.3	1.242	8.960	52.627	52.627	0.04869	-0.129	0.666	-34.50	12.53	0.345
56	24	0.84	-155.1	95.6	1.247	7.828	188.612	188.612	0.02572	-0.815	0.665	-1.47	11.34	0.382

SIMULATION MODEL OF BARE SOIL EVAPORATION IN DESERTS (E V A D E S)
version march 1988

outputfile :EVADES.ACT

day	hour	rhoair	vpd	sa	ss	rav	rah	ri	rnrad	totheat	ge	rsh	psych	rs/	rle0	temp(1)	rh
-	-	kg.m-3	mbar	mbar.k-1	s.m-1	s.m-1	s.m-1	-	w.m-2	w.m-2	w.m-2	s.m-1	mbar.k-1	s.m-1	w.m-2	c	-

HOMOGENEOUS SALINE SAND PROFILE, SUMMERPERIOD, QATTARA DEPRESSION

56	1	1.251	7.0	0.80	1.78	271.08	271.07856	-1.30851	-149.3	-13.0	347.2	0.6245E-03	0.664	0.6551	-124.	10.497	0.418
56	1	1.251	7.0	0.80	1.78	271.08	271.07856	-1.30851	-149.3	0.0	347.2	0.2206E-02	0.664	2.815	-132.	10.497	0.418
56	2	1.252	6.3	0.77	1.68	311.70	311.69667	-1.56669	-142.6	1.3	-144.6	0.2764E-01	0.664	23.65	133.	10.056	0.455
56	3	1.252	5.9	0.77	1.57	311.70	311.70324	-1.56673	-134.9	2.4	-40.0	0.4741E-01	0.664	45.37	66.3	10.056	0.491
56	4	1.250	5.7	0.80	1.45	271.10	271.09838	-1.30863	-126.2	3.6	-3.7	0.9554E-01	0.664	1071.	16.2	10.497	0.527
56	5	1.240	6.0	0.90	1.32	52.69	52.68661	-0.12927	-113.6	5.0	0.1	0.1130	0.666	787.1	-2.95	12.526	0.564
56	6	1.227	6.6	1.07	1.20	119.55	119.54919	0.56683	-98.7	5.9	2.7	0.1264	0.668	468.5	3.97	15.500	0.600
56	7	1.206	9.6	1.38	1.81	139.17	139.17002	0.69157	84.9	-23.6	-2.4	0.1456	0.671	445.0	-24.5	20.167	0.569
56	8	1.187	13.4	1.75	2.61	156.51	156.51117	0.80556	217.2	-23.8	-7.8	0.1599	0.673	443.8	-53.5	24.562	0.538
56	9	1.170	18.0	2.13	3.53	170.99	170.99056	0.90321	355.3	-21.6	-11.9	0.1768	0.676	588.0	-80.4	28.431	0.508
56	10	1.157	22.8	2.49	4.47	182.18	182.18264	0.98013	505.2	-17.8	-67.0	0.1806	0.678	433.3	-85.3	31.548	0.477
56	11	1.153	25.9	2.64	4.88	186.45	186.44984	1.00978	627.2	-7.0	-72.9	0.1806	0.679	418.6	-117.	32.766	0.446
56	12	1.149	28.8	2.77	5.24	189.79	189.79448	1.03313	689.8	-5.5	-77.5	0.1806	0.679	408.3	-132.	33.733	0.415
56	13	1.147	31.6	2.86	5.50	192.20	192.19709	1.04997	684.3	-4.0	-80.9	0.1806	0.680	401.0	-130.	34.433	0.385
56	14	1.146	33.9	2.92	5.64	193.64	193.64414	1.06014	610.9	-1.1	-81.7	0.1806	0.680	397.5	-113.	34.858	0.354
56	15	1.147	35.5	2.92	5.67	193.64	193.64488	1.06014	479.8	-1.3	-82.9	0.1806	0.680	396.8	-77.8	34.858	0.323
56	16	1.152	34.9	2.77	5.38	189.80	189.79668	1.03315	316.4	0.8	-82.9	0.1806	0.679	405.1	-34.2	33.733	0.292
56	17	1.161	32.2	2.49	4.72	182.19	182.18526	0.98016	151.0	7.2	-77.5	0.1806	0.678	419.8	1.60	31.549	0.262
56	18	1.175	28.1	2.13	3.84	171.00	170.99550	0.90325	12.2	13.2	-67.0	0.1805	0.676	434.2	23.2	28.432	0.231
56	19	1.191	23.3	1.75	2.81	156.52	156.51731	0.80561	-149.3	18.8	-52.1	0.1804	0.673	444.4	41.8	24.563	0.200
56	20	1.229	12.7	1.07	1.96	439.75	439.75214	1.57454	-177.3	59.3	1.7	0.1802	0.668	406.2	26.0	15.500	0.236
56	21	1.229	12.1	1.07	1.96	439.75	439.75214	1.57454	-168.9	-5.2	-5.8	0.1802	0.668	432.5	48.5	15.500	0.273
56	22	1.236	10.4	0.98	1.94	231.65	231.65060	0.69040	-164.6	-4.2	-12.0	0.1803	0.667	458.3	29.7	13.951	0.309
56	23	1.242	9.0	0.90	1.91	52.63	52.62685	-0.12903	-160.1	-2.9	-16.5	0.1803	0.666	482.1	5.29	12.527	0.345
56	24	1.247	7.8	0.84	1.86	188.61	188.61177	-0.81494	-155.1	-1.2	-18.8	0.1803	0.665	504.7	24.8	11.343	0.382

SIMULATION MODEL OF BARE SOIL EVAPORATION IN DESERTS (E V A D E S)
version march 1988

outputfile :EVADES.VAP1

day	time	ts/	lab.th	lab.sp	a(1)	velocity	evmax	evact	airratio	temp	virt.temp.	rhoair	dens	vap.flux
-	-	-	w.m J.k-1		m2.s-1	m.s-1	mbar	mbar	-	c	k	kg.m-3	kg.m-3	kg.m-2.s-1

UNDISTURBED SALINE SAND PROFILE, SUMMERPERIOD, QATTARA DEPRESSION

87	1	1	0.32	1.68	0.150E-05	0.114	28.85	0.34	0.206E-03	24.44	297.69	1.194	0.246E-03	0.281E-04
87	1	2	0.32	1.68	0.150E-05	0.115	31.06	0.35	0.212E-03	25.68	298.87	1.189	0.252E-03	0.289E-04
87	1	3	0.32	1.68	0.150E-05	0.115	33.41	0.36	0.218E-03	26.92	300.11	1.184	0.258E-03	0.296E-04
87	1	4	0.32	1.68	0.150E-05	0.115	30.57	0.31	0.191E-03	25.41	298.59	1.190	0.227E-03	0.260E-04
87	1	5	0.31	1.68	0.150E-05	0.114	27.95	0.28	0.171E-03	23.90	297.08	1.196	0.204E-03	0.233E-04
87	1	6	0.31	1.68	0.150E-05	0.114	26.45	0.26	0.162E-03	22.99	296.17	1.200	0.194E-03	0.220E-04
87	1	7	0.31	1.68	0.150E-05	0.114	25.95	0.26	0.158E-03	22.68	295.85	1.201	0.190E-03	0.216E-04
87	1	8	0.31	0.24	0.210E-06	0.562E-07	25.46	0.25	0.155E-03	22.36	295.54	1.203	0.187E-03	0.105E-10
87	1	9	0.31	0.25	0.226E-06	0.827E-07	24.98	0.25	0.152E-03	22.04	295.22	1.204	0.184E-03	0.152E-10
87	1	10	0.31	0.27	0.241E-06	0.728E-07	24.50	0.24	0.150E-03	21.73	294.90	1.205	0.180E-03	0.131E-10
87	1	11	0.31	0.30	0.269E-06	0.719E-07	24.16	0.24	0.148E-03	21.50	294.68	1.206	0.178E-03	0.128E-10
87	1	12	0.31	0.35	0.309E-06	0.280E-02	23.96	0.24	0.146E-03	21.36	294.54	1.207	0.176E-03	0.494E-06
87	1	13	0.31	0.39	0.350E-06	0.652E-02	23.76	0.24	0.145E-03	21.22	294.40	1.207	0.175E-03	0.114E-05
87	1	14	0.31	0.44	0.390E-06	0.102E-01	23.56	0.24	0.144E-03	21.09	294.26	1.208	0.174E-03	0.178E-05
87	1	15	0.31	0.48	0.430E-06	0.139E-01	23.36	0.23	0.143E-03	20.95	294.12	1.208	0.172E-03	0.240E-05
87	1	16	0.31	0.48	0.430E-06	0.139E-01	23.16	0.23	0.141E-03	20.81	293.99	1.209	0.171E-03	0.238E-05
87	1	17	0.31	0.48	0.430E-06	0.139E-01	22.97	0.23	0.140E-03	20.67	293.85	1.209	0.170E-03	0.237E-05
87	1	18	0.31	0.48	0.430E-06	0.139E-01	22.77	0.23	0.139E-03	20.53	293.71	1.210	0.168E-03	0.235E-05
87	1	19	0.31	0.48	0.430E-06	0.139E-01	22.58	0.01	0.528E-05	20.40	293.55	1.211	0.640E-05	0.889E-07
87	1	20	0.31	0.48	0.430E-06	0.141E-01	22.39	20.40	0.127E-01	20.26	295.65	1.202	0.153E-01	0.216E-03
87	1	21	2.76	1.04	0.430E-06	0.205E-02	21.86	21.38	0.133E-01	19.87	295.37	1.203	0.160E-01	0.328E-04
87	2	1	0.31	1.68	0.150E-05	0.114	26.81	0.30	0.185E-03	23.21	296.40	1.199	0.222E-03	0.252E-04
87	2	2	0.32	1.68	0.150E-05	0.114	29.37	0.31	0.189E-03	24.73	297.92	1.193	0.226E-03	0.258E-04
87	2	3	0.32	1.68	0.150E-05	0.115	32.13	0.32	0.196E-03	26.25	299.44	1.187	0.233E-03	0.267E-04
87	2	4	0.32	1.68	0.150E-05	0.114	29.58	0.30	0.181E-03	24.85	298.04	1.192	0.215E-03	0.246E-04
87	2	5	0.31	1.68	0.150E-05	0.114	27.20	0.27	0.164E-03	23.46	296.64	1.198	0.199E-03	0.227E-04
87	2	6	0.31	1.68	0.150E-05	0.114	25.86	0.26	0.156E-03	22.61	295.79	1.202	0.190E-03	0.215E-04
87	2	7	0.31	1.68	0.150E-05	0.113	25.41	0.25	0.155E-03	22.33	295.51	1.203	0.187E-03	0.212E-04
87	2	8	0.31	0.24	0.210E-06	0.249E-06	24.98	0.25	0.152E-03	22.04	295.22	1.204	0.184E-03	0.456E-10
87	2	9	0.31	0.25	0.226E-06	0.827E-07	24.54	0.25	0.150E-03	21.76	294.93	1.205	0.181E-03	0.149E-10
87	2	10	0.31	0.27	0.241E-06	-.101E-06	24.12	0.24	0.147E-03	21.47	294.65	1.206	0.178E-03	-.179E-10
87	2	11	0.31	0.30	0.269E-06	0.718E-07	23.82	0.24	0.145E-03	21.27	294.44	1.207	0.176E-03	0.126E-10
87	2	12	0.31	0.35	0.309E-06	0.280E-02	23.64	0.24	0.144E-03	21.15	294.32	1.208	0.174E-03	0.489E-06
87	2	13	0.31	0.39	0.350E-06	0.652E-02	23.47	0.23	0.143E-03	21.02	294.20	1.208	0.173E-03	0.113E-05
87	2	14	0.31	0.44	0.390E-06	0.102E-01	23.29	0.23	0.142E-03	20.90	294.08	1.209	0.172E-03	0.176E-05
87	2	15	0.31	0.48	0.430E-06	0.139E-01	23.12	0.23	0.141E-03	20.78	293.96	1.209	0.171E-03	0.238E-05
87	2	16	0.31	0.48	0.430E-06	0.139E-01	22.95	0.23	0.140E-03	20.66	293.83	1.210	0.169E-03	0.236E-05
87	2	17	0.31	0.48	0.430E-06	0.139E-01	22.77	0.23	0.139E-03	20.54	293.71	1.210	0.168E-03	0.235E-05
87	2	18	0.31	0.48	0.430E-06	0.139E-01	22.60	0.23	0.138E-03	20.41	293.59	1.211	0.167E-03	0.233E-05
87	2	19	0.31	0.48	0.430E-06	0.139E-01	22.43	0.01	0.385E-05	20.29	293.44	1.211	0.466E-06	0.648E-07
87	2	20	0.31	0.48	0.430E-06	0.141E-01	22.27	20.24	0.126E-01	20.17	295.55	1.203	0.152E-01	0.214E-03
87	2	21	2.76	1.04	0.430E-06	0.203E-02	21.80	21.32	0.133E-01	19.83	295.32	1.203	0.160E-01	0.325E-04
87	3	1	0.31	1.68	0.150E-05	0.113	24.71	0.27	0.165E-03	21.87	295.05	1.205	0.199E-03	0.226E-04
87	3	2	0.31	1.68	0.150E-05	0.114	27.15	0.28	0.169E-03	23.42	296.60	1.198	0.202E-03	0.230E-04
87	3	3	0.32	1.68	0.150E-05	0.114	29.79	0.30	0.182E-03	24.97	298.16	1.192	0.217E-03	0.248E-04
87	3	4	0.31	1.68	0.150E-05	0.114	27.75	0.28	0.169E-03	23.79	296.97	1.197	0.203E-03	0.231E-04
87	3	5	0.31	1.68	0.150E-05	0.114	25.83	0.26	0.158E-03	22.60	295.78	1.202	0.189E-03	0.215E-04
87	3	6	0.31	1.68	0.150E-05	0.113	24.74	0.25	0.151E-03	21.89	295.07	1.204	0.182E-03	0.208E-04
87	3	7	0.31	1.68	0.150E-05	0.113	24.40	0.24	0.147E-03	21.66	294.84	1.205	0.180E-03	0.203E-04
87	3	8	0.31	0.24	0.210E-06	-.836E-07	24.07	0.24	0.147E-03	21.44	294.61	1.206	0.177E-03	-.148E-10
87	3	9	0.31	0.25	0.226E-06	0.660E-07	23.73	0.24	0.145E-03	21.21	294.38	1.207	0.175E-03	0.116E-10
87	3	10	0.31	0.27	0.241E-06	0.252E-02	23.41	0.23	0.143E-03	20.98	294.16	1.208	0.173E-03	0.436E-06
87	3	11	0.31	0.30	0.269E-06	0.640E-07	23.18	0.23	0.141E-03	20.82	294.00	1.209	0.171E-03	0.110E-10
87	3	12	0.31	0.35	0.309E-06	0.282E-02	23.05	0.23	0.141E-03	20.73	293.91	1.209	0.170E-03	0.480E-06
87	3	13	0.31	0.39	0.350E-06	0.653E-02	22.92	0.23	0.140E-03	20.64	293.81	1.210	0.169E-03	0.111E-05
87	3	14	0.31	0.44	0.390E-06	0.102E-01	22.79	0.23	0.139E-03	20.55	293.72	1.210	0.168E-03	0.172E-05
87	3	15	0.31	0.48	0.430E-06	0.139E-01	22.66	0.23	0.138E-03	20.46	293.63	1.210	0.167E-03	0.234E-05
87	3	16	0.31	0.48	0.430E-06	0.139E-01	22.54	0.23	0.138E-03	20.37	293.54	1.211	0.167E-03	0.232E-05
87	3	17	0.31	0.48	0.430E-06	0.139E-01	22.41	0.22	0.137E-03	20.27	293.45	1.211	0.166E-03	0.231E-05
87	3	18	0.31	0.48	0.430E-06	0.139E-01	22.28	0.22	0.136E-03	20.18	293.36	1.211	0.165E-03	0.230E-05
87	3	19	0.31	0.48	0.430E-06	0.139E-01	22.16	0.01	0.363E-05	20.09	293.24	1.212	0.427E-06	0.594E-07

```
HOMOGENEOUS SALINE SAND PROFILE, SUMMERPERIOD, QATTARA DEPRESSION, EGYPT
56 76 28 1 1
56 76 0.0416666 1.0 0.1
1 220 1 40 2 40 40 40 40 40
1.3
18. 0.7
0.01
0.37
1.00
1 220
1.3 1.3
0.5000E+08 0.6500E+03 0.3550E+03 0.2460E+03 0.1850E+03 0.1520E+03 0.1290E+03
0.1100E+03 0.9500E+02 0.7800E+02 0.7100E+02 0.6500E+02 0.6000E+02 0.5600E+02
0.5100E+02 0.4900E+02 0.4500E+02 0.4200E+02 0.3900E+02 0.3500E+02 0.3300E+02
0.3100E+02 0.2900E+02 0.2700E+02 0.2500E+02 0.2400E+02 0.2200E+02 0.2100E+02
0.1900E+02 0.1750E+02 0.1600E+02 0.1450E+02 0.1250E+02 0.1100E+02 0.9000E+01
0.6500E+01 0.2500E+01
0.159E-08 0.318E-04 0.166E-03 0.489E-03 0.105E-02 0.178E-02 0.262E-02
0.411E-02 0.615E-02 0.953E-02 0.134E-01 0.165E-01 0.197E-01 0.251E-01
0.305E-01 0.32 E-01 0.407E-01 0.475E-01 0.508E-01 0.711E-01 0.820E-01
0.890E-01 0.925E-01 0.97E-01 0.140 0.16 0.17 0.185
0.195 0.220 0.244 0.275 0.315 0.36 0.421
0.5115 0.6885
38.
3 5 2 2
0 2 0.24 0.10
0 0.2 0.6
0 0.2 0.6
0 0.2 0.6
0 0.2 0.6
0 0.2 0.6
0 0.2 0.6
0 0.2 0.6
0 0.2 0.6
0 0.2 0.6
0 0.2 0.6
0 0.2 0.6
0 0.2 0.6
0 0.2 0.6
0 0.2 0.6
0 0.2 0.6
0 0.2 0.6
0 0.2 0.6
0 0.2 0.6
0 0.2 0.6
0 0.2 0.6
0 0.2 0.6
20 170 330
2.5 5.0 10.0 24.0 40.0
10 40
100 200
6.00 19.00 25.0 25.0
1100.0 0.0 0.0
51.8 32.0 17.0
35.0 33.0 31.0
10.0 11.0 12.0
15.5 14.5 12.5
47. 40. 32. 28.0 21.9
27. 23.2 21.6 20.2 18.9
18.7 18.3 18.6 19.2 19.9
1.6 1.8
```